Bio-Sciences, Uppsala, Sweden). The protein solution (200 μg proteins) was incubated with 40 mM dithiothreitol at 65° for 30 min. Freshly prepared sodium iodoacetate (final concentration, 96 mM) was added to the sample solution, and the mixture was incubated at room temperature for 40 min in the dark. The reaction was stopped by adding cystine (6 mg/ml in 2 M HCl) in an amount equal to the amount of dithiothreitol. The solution containing carboxymethylated proteins was diluted in four times its volume of H_2O, and the mixture was incubated with 0·1 μg of thermolysin at 65° for 1 hr. After terminating the reaction by boiling, the reaction mixture was diluted in four times its volume of 0·2 M acetate buffer. The *N*-linked glycans were released by treatment with PNGase A (1 mU) at 37° for 16 hr and were desalted using an EnviCarb C cartridge (Supelco, Bellefonte, PA).

Labelling of N-glycans with d_0-AP and d_6-AP

Glycans released from the SLE-model mouse cells were incubated in acetic acid (20 μl) with 12·5 M d_0-AP at 90° for 1 hr. Next, 3·3 M borane–dimethylamine complex reducing reagent in acetic acid (20 μl) was added to the solution and the mixture was incubated at 80° for 1 hr. Excess reagent was removed by evaporation, and d_0-PA glycans were desalted using an EnviCarb C cartridge, concentrated in a SpeedVac and reconstituted in 20 μl of 5 mM ammonium acetate (pH 9·6). Glycans released from the control mouse were labelled with d_6-AP in a similar manner. The resulting d_4-PA glycans were combined with d_0-PA glycans, which were prepared from an equal amount of proteins.

On-line liquid chromatography/mass spectrometry

The sample solution (4 μl) was injected into the LC/MS system through a 5-μl capillary loop. The d_0-PA and d_4-PA glycans were separated in a graphitized carbon column (Hypercarb, 150 × 0·2 mm, 5 μm; Thermo Fisher Scientific, Waltham, MA) at a flow rate of 2 μl/min in a Magic 2002 LC system (Michrom Bioresources, Auburn, CA). The mobile phases were 5 mM ammonium acetate containing 2% acetonitrile (pH 9·6, A buffer) and 5 mM ammonium acetate containing 90% acetonitrile (pH 9·6, B buffer). The PA-glycans were eluted with a linear gradient of 5–45% of B buffer for 90 min.

Mass spectrometric analysis of PA glycans was performed using a Fourier transform ion cyclotron resonance/ion trap mass spectrometer (FT-ICR-MS, LTQ-FT; Thermo Fisher Scientific) equipped with a nanoelectrospray ion source (AMR, Tokyo, Japan). For MS, the electrospray voltage was 2·0 kV in the positive ion mode, the capillary temperature was 200°, the collision energy was 25% for MS^n experiment, and the maximum injection times for FT-ICR-MS and MS^n were 1250 and 50 milliseconds, respectively. The resolution of FT-ICR-MS was 50 000, the scan time (*m/z* 700–2000) was approximately 0·2 seconds, dynamic exclusion was 18 seconds, and the isolation width was 3·0 U (range of precursor ions ± 1·5).

Results

Quantitative profiling of kidney oligosaccharides in the SLE-model mouse

The recovery of oligosaccharides from whole tissues and cells is generally low because of the insolubility of the membrane fraction and possible degradation of the glycans. To improve the recovery of *N*-glycans from kidney cells, whole cells were dissolved in guanidine hydrochloride solution, and all proteins, including membrane proteins, were digested into peptides and glycopeptides with thermolysin. The *N*-glycans were then released from the glycopeptides with PNGase A, which is capable of liberating *N*-linked oligosaccharides even at the N- and/or C-terminals of peptides. The *N*-linked oligosaccharides from the SLE-model mice and control mice were labelled with d_0-AP and d_6-AP, respectively. The mixture of labelled glycans derived from an equal amount of proteins was subjected to quantitative glycan profiling using LC/MS^n.

Figure 1(b) shows the total ion chromatogram obtained by a single mass scan (*m/z* 700–2000) of the glycan mixture in the positive ion mode. Although the MS data contain many MS spectra derived from contaminating low-molecular-weight peptides, the MS/MS spectra of oligosaccharides could be sorted based on the existence of carbohydrate-distinctive ions, such as $HexHexNAc^+$ (*m/z* 366) and $Hex(dHex)HexNAc^+$ (*m/z* 512). The monosaccharide compositions of the precursor ions were calculated from accurate *m/z* values acquired by FT-ICR-MS. Oligosaccharides found at 25–27 min were assigned to low-molecular-mass glycans consisting of $dHex_{0,1}Hex_{4,3}HexNAc_2$ (dHex, deoxyhexose; Hex, hexose; HexNAc, *N*-acetylhexosamine). High-mannose-type glycans, which consist of $Hex_{5-10}HexNAc_2$, were located at 20–28 min; complex-type glycans ($dHex_{0-3}Hex_{3-6}HexNAc_{4-6}$) were found at 21–27 min. Figure 2(a) shows the relative intensities of the molecular ions of *N*-glycans in the SLE-model mouse, which may correspond roughly to the levels of individual *N*-glycans. More than half of all glycans were complex-type oligosaccharides, and the most prominent glycan was $dHex_3Hex_5HexNAc_5$. Man-9 ($Hex_9HexNAc_2$) was the second most common oligosaccharide. Nearly one-quarter of the glycans were low-molecular-mass glycans, and $dHex_1Hex_2HexNAc_2$ was the third most abundant glycan in the SLE-model mouse. The rate of percentage change in individual glycans between the SLE-model mice and control mice was calculated from the intensity ratio of d_0-glycan and d_4-glycan

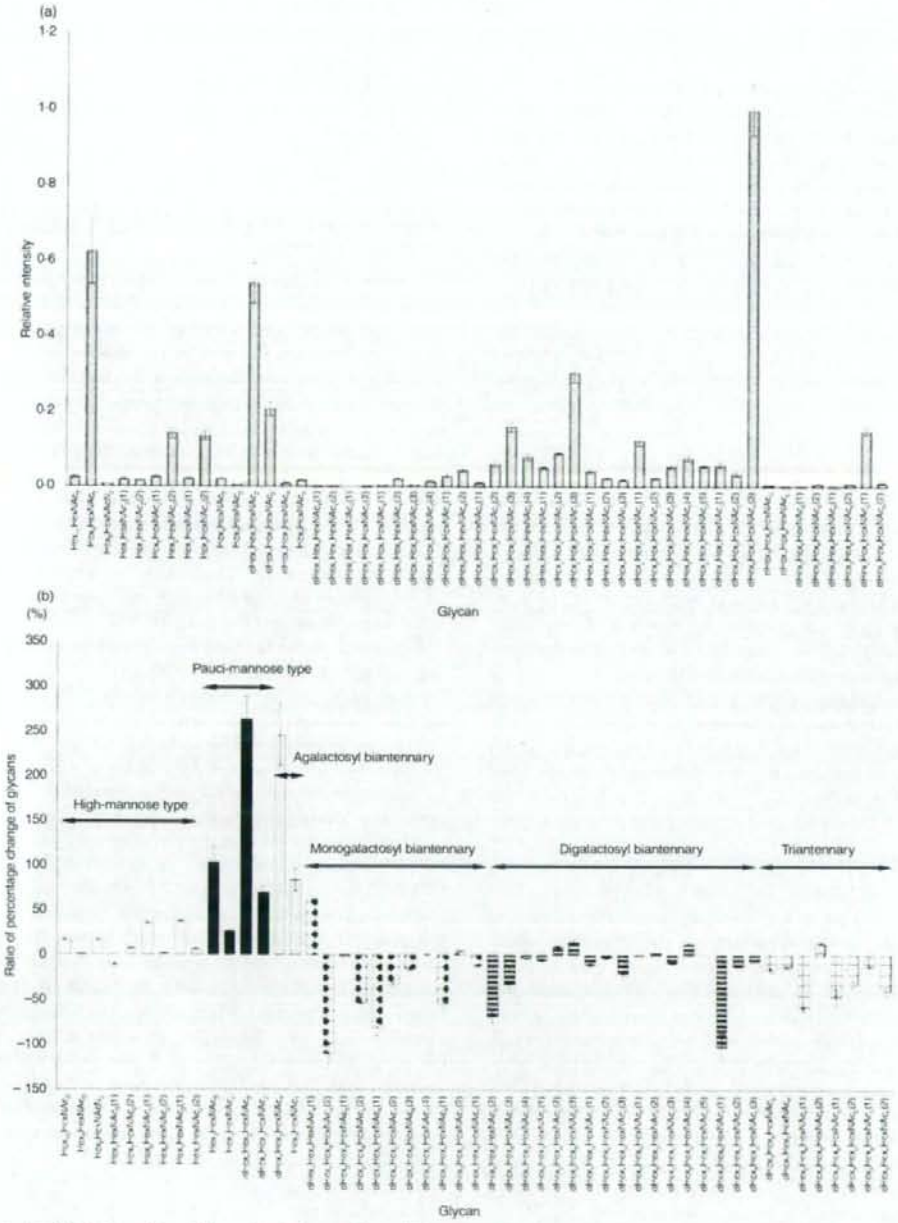

Figure 2. (a) Relative intensities of the molecular ions of d_0-pyridyl amino (PA) glycans from the systemic lupus erythematosus (SLE) model mouse. The intensity of the most intense ion $([M + 2H]^{2+}$ of d_4-PA $dHex_3Hex_5HexNAc_3(3)$, *m/z* 1180·97) was taken as 1·0. (b) Rate of percentage change of d_0/d_4-glycans. Each value is the average of three biological repeats. Error bars correspond to the standard deviation. The numbers in parentheses show the isomers.

molecular ions (Fig. 2b). The significant changes found in many glycans are described below.

Increased oligosaccharides in the SLE-model mouse

Figure 3(a,b) show the mass and MS/MS spectra of the most increased glycan, which showed a notable increase in the SLE-model mouse. Based on *m/z* values of molecular ions and differences of 1·00 U in *m/z* values among monoisotopic ions, the intense ion (*m/z* 973·40) and its neighbour ion (*m/z* 977·43) were assigned to $[M+H]^+$ of d_0-PA $dHex_1Hex_2HexNAc_2$, and d_4-PA $dHex_1Hex_2HexNAc_2$, respectively (Fig. 3a). The intensity ratio of these ions suggested that the level of $dHex_1Hex_2HexNAc_2$ increased 3·6-fold in the SLE-model mouse. The structure of this oligosaccharide was estimated to be a core-fucosylated trimannosyl core lacking a Man residue from the successive cleavages of Man (Y_3: *m/z* 815), Man (Y_2: *m/z* 653), GlcNAc (Y_1: *m/z* 450) and Fuc ($Y_{1/1'}$: *m/z* 304) (inset in Fig. 3b). Such a defective *N*-glycan is known as a paucimannose-type glycan, and is rarely found in vertebrates. All paucimannose-type glycans, such as $dHex_1Hex_3HexNAc_2$ (a core-fucosylated trimannosyl core) and $Hex_3HexNAc_2$ (a non-fucosylated trimannosyl core) were increased in the SLE-model mouse. Furthermore, a two-fold increase was found in $Hex_4HexNAc_2$ (Man-4).

Figure 4 shows the molecular ratios of individual *N*-glycans between the SLE-model mice and control mice. A remarkable increase (3·5-fold) was also found in $dHex_1Hex_3HexNAc_4$, which is assigned to a core-fucosylated biantennary oligosaccharide lacking two non-reducing terminal Gal residues; its non-fucosylated form ($Hex_3HexNAc_4$) was also increased 1·8-fold in the SLE-model mouse. In other complex-type glycans, $dHex_1Hex_4HexNAc_4$ (1), which is assigned to a biantennary oligosaccharide lacking one molecule of Gal, increased 1·6-fold. Interestingly, a significant decrease was found in $dHex_1Hex_4HexNAc_4$ (2), a positional isomer of $dHex_1Hex_4HexNAc_4$ (1); this might have been caused by galactosylation on either GlcNAc-Manα1–3 or GlcNAc-Manα1–6. In contrast, no change was found between fucosylated and non-fucosylated oligosaccharides, nor between bisected and non-bisected oligosaccharides.

A significant increase was found in some high-mannose-type oligosaccharides, such as $Hex_5HexNAc_2$ (Man-5; + 137%) and $Hex_6HexNAc_2$ (1) (Man-6; + 136%), while $Hex_7HexNAc_2$ (1,2) (Man-7) and a positional isomer of $Hex_6HexNAc_2$ (1) [$Hex_6HexNAc_2$ (2)] remained unchanged in the SLE-model mouse. A slight increase was found in $Hex_8HexNAc_2$ (Man-8; + 116%) and $Hex_{10}HexNAc_2$ (possibly assigned to Man-9 plus Glc; + 116%).

Decreased oligosaccharides in the SLE-model mouse

The mass spectrum of the most decreased glycan is shown in Fig. 5(a). Based on differences of 0·5 U in *m/z* values among monoisotopic ions, molecular ions at *m/z* 1180·97

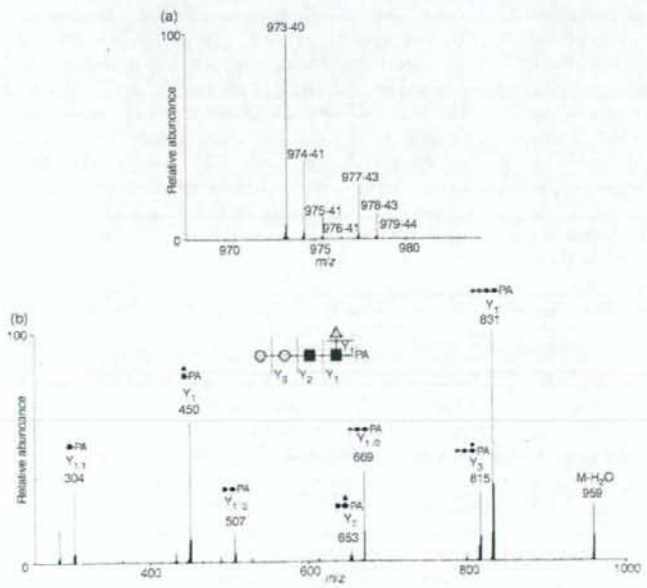

Figure 3. Mass (a) and mass spectrometry (MS)/MS (b) spectra of the most increased glycan ($dHex_1Hex_2HexNAc_2$). Precursor ion, *m/z* 973·4; grey circle, mannose; grey triangle, fucose; black square, *N*-acetylglucosamine.

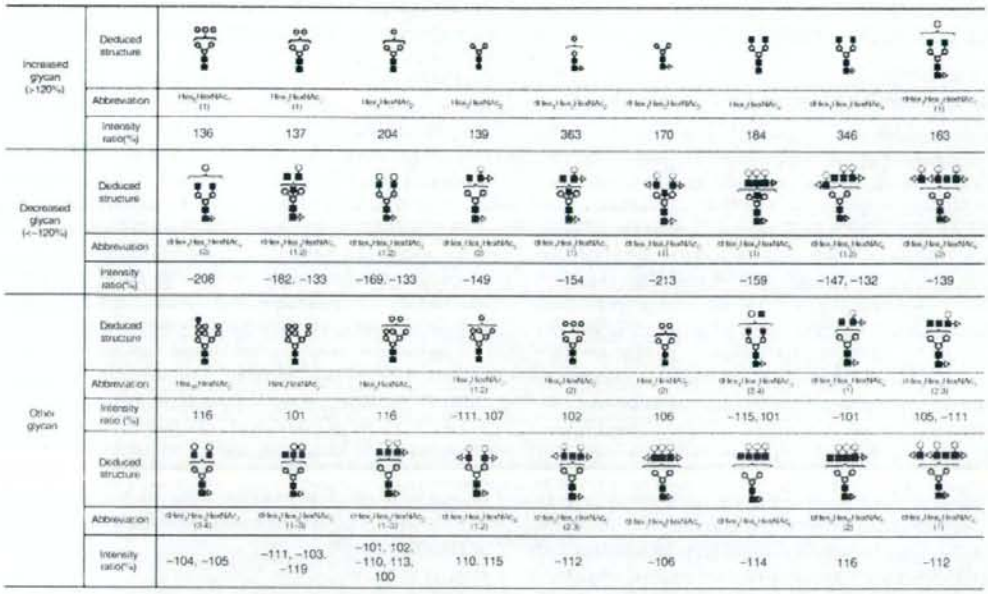

Figure 4. Summary of quantitative analysis of the systemic lupus erythematosus (SLE) model mouse against control mice. Values of relative ratios are the averages of three biological repeats. Grey circle, mannose; white circle, galactose; grey triangle, fucose; black square, *N*-acetylglucosamine.

and 1182·98 are estimated to be $[M + 2H]^{2+}$ of d_0-PA and d_4-PA $dHex_3Hex_5HexNAc_5$ (1), respectively. The intensity ratio of $d_0 : d_4$ glycans suggests that this glycan in the SLE-model mouse was decreased to 47% of the amount found in the control mouse. Figure 5(b) shows the MS^{2-4} spectra of d_0-PA $dHex_3Hex_5HexNAc_5$ (1) (precursor ion, *m/z* 1180·97). The fragment ion at *m/z* 512 in MS/MS (i) and MS/MS/MS (ii) spectra, which corresponds to $dHex_1Hex_1HexNAc_1^+$, suggests the attachment of two Lewis motifs on the side chains of the glycan. The presence of $dHex_1HexNAc_1PA^+$ (*m/z* 446) and $dHex_1Hex_1HexNAc_3PA^+$ (*m/z* 1015) reveals the linkages of a core fucose and a bisecting GlcNAc. Based on these fragments, this decreased glycan is estimated to be a Lewis-motif-modified, core-fucosylated and bisected biantennary oligosaccharide (inset in Fig. 5).

As shown in Figs 2(b) and 4, oligosaccharides lacking one molecule of Gal with and without bisecting GlcNAc [$dHex_1Hex_4HexNAc_4$ (2) and $dHex_1Hex_4HexNAc_5$ (1)] were decreased to 48% and 55%, respectively. A significant decrease was also found in other monogalactobiantennary oligosaccharides, such as $dHex_3Hex_4HexNAc_4$ (2) (a Lewis-motif-modified, core-fucosylated monogalacto-biantennary) and $dHex_2Hex_4HexNAc_5$ (1) (a Lewis-motif-modified core-fucosylated and bisected monogalacto-biantennary).

The oligosaccharides, non-reducing ends of which are fully galactosylated, were decreased in the SLE-model mouse. For example, monofucosyl biantennary $dHex_1Hex_3HexNAc_4$ (1) and (2) were decreased 59% and 75%, respectively. The di-, tri- and tetra-fucosylated oligosaccharides, $dHex_2Hex_6HexNAc_6$ (1), $dHex_3Hex_6HexNAc_6$ (1,2) and $dHex_4Hex_6HexNAc_6$ (1,2), which were estimated to be tri- and tetraantennary forms, were also significantly decreased. These results show that oligosaccharides with a complicated structure, such as high branching oligosaccharides and di- and tri-fucosylated oligosaccharides, were decreased in the SLE-model mouse.

Discussion

Using the isotope-tagging method, we demonstrated aberrant *N*-glycosylation on the kidney proteins of a SLE-model mouse. We found increases in low-molecular-mass glycans with simple structures, including paucimannose-type glycans, agalacto-biantennary oligosaccharides, Man-5 and Man-6, and decreases in glycans which have a complicated and diverse structure, such as digalacto-biantennary oligosaccharides and highly fucosylated glycans (Fig. 4). An increase in agalacto-biantennary oligosaccharides on IgG has been reported in the sera of patients with autoimmune diseases, including SLE, rheumatoid arthritis and IgA

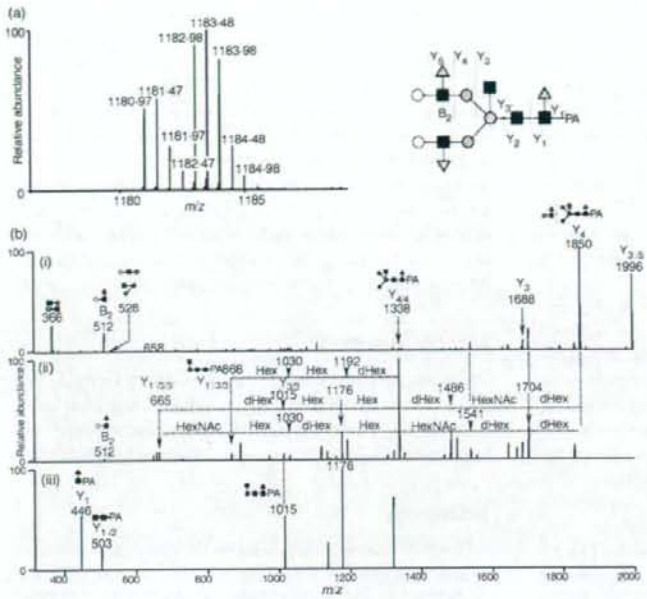

Figure 5. (a) Mass spectrum of the most decreased glycan [$dHex_4Hex_3HexNAc_5$ (11)]; (b-i) Mass spectrometry (MS)/MS spectrum of *m/z* 1181·0; (b-ii) MS/MS/MS spectrum of *m/z* 1849·7; (b-iii) MS/MS/MS/MS spectrum of *m/z* 1338·3. Grey circle, mannose; white circle, galactose; grey triangle, fucose; black square, *N*-acetylglucosamine; dHex, deoxyhexose (fucose); Hex, hexose (mannose and galactose); HN, *N*-acetylhexosamine (*N*-acetylglucosamine).

nephropathy.[9,11,28] The present findings show that abnormal glycosylation occurs not only in IgG in serum but also in several glycoproteins in the SLE-model mouse kidney.

Figure 6 shows the biosynthesis pathway of *N*-linked oligosaccharides in mammalian cells. Man-9, a product in the early stage of the pathway, is processed to Man-5 in the endoplasmic reticulum, and a GlcNAc and Fuc are added to Man-5 in the Golgi apparatus. After the removal of two Man residues by αM-II, GlcNAc, Gal and Fuc are further added to oligosaccharides by several glycosyltransferases. There have been a few reports on paucimannose-type oligosaccharides in vertebrates;[29] however, these glycans are common oligosaccharides in other multicellular organisms such as insects and *Caenorhabditis elegans*.[30,31] The membrane protease β-*N*-acetylglucosaminidase is thought to mediate the synthesis of paucimannose-type oligosaccharides.[32] Based on core fucosylation on some paucimannose-type oligosaccharides, it was deduced that β-*N*-acetylglucosaminidase might act on glycan synthesis after *N*-acetylglucosaminyltransferase I, core fucosyltransferase and αM-II.[32] The synthesis of paucimannose-type oligosaccharides may be involved in the suppression of growing diversity and complexity of glycan structures.

We found a number of changes in the levels of monogalacto-biantennary oligosaccharides in the SLE mouse. Galactosylation to agalacto-biantennary oligosaccharides is mediated by β-1,4-galactosyltransferase

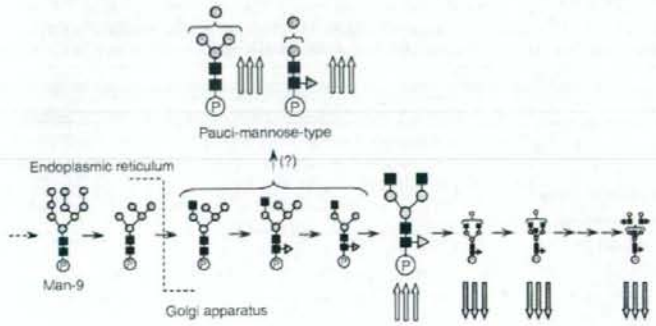

Figure 6. Biosynthesis pathway of *N*-linked oligosaccharides in mammalian cells. Triple up-arrow, increases of more than +2·0; triple down-arrow, decreases of not more than −2·0. Grey circle, mannose; white circle, galactose; grey triangle, fucose; black square, *N*-acetylglucosamine. 'P' is protein portion.

(β-1,4-GalTase).[33] Previous studies suggested that translational repression of β-1,4-GalTase in lymphocytes is associated with an increase in agalacto-oligosaccharides on IgG in the serum of the MRL-lpr mouse.[34] Although the activity of β-1,4-GalTase remains unknown in the SLE-model mouse, the increase in agalacto forms and the decrease in digalacto forms imply changes in β-1,4-GalTase activity. The present results suggest a decrease in diverse and complex glycans, which are synthesized at a late stage in the *N*-glycan synthesis pathway, and an increase in the simple glycans appearing at an early stage in the SLE-model mouse.

The activation of complements is involved in glomerular nephritis of SLE.[35–37] The complements are activated through three pathways: a classical pathway, an alternative pathway and a lectin pathway. In the classical pathway, a binding of C1q to an immune complex triggers the activation of C1r and C1s. Activated C1s cleaves C4 and C2, generating C3 convertase (C4b2a), which generates C3b. The complement component subsequently produces C5b-9 complex, which leads to an inflammatory response on host tissues.[38–41] The excess deposition of immune complexes followed by a sustained immune response triggers tissue disorders, including lupus nephritis.[42–45] In the lectin pathway, mannose-binding lectin (MBL) is associated with the activation of complements. Two forms of MBL (MBL-A and MBL-C) are present in complexes with MBL-associated serine proteases (MASPs) in mice. The MASPs are activated by binding MBL to Man or GlcNAc on the surface of the antigen in a calcium-dependent manner.[46–49] Like C1s in the classical pathway, activated MASPs cleave C4 and C2.[50,51] In lupus nephritis, MBL-A and MBL-C in the immune complex bind to GlcNAc residues at the reducing ends of agalacto-biantennary oligosaccharides in IgG,[52] and subsequently activate the complements.[53,54] In αM-II-deficient mice, which suffer from SLE-like syndromes including kidney disorders, the majority of glycans are hybrid-type oligosaccharides because of the failure of Man trimming by the lack of αM-II.[16] Green *et al.* concluded that MBL recognized Manα1–3 and Manα1–6 linkages in hybrid-type oligosaccharides,[17] and glycans lacking normal side chains, including agalacto-biantennary oligosaccharides, might be involved in the aberrant immune response in autoimmune diseases. Paucimannose glycans, which contain exposed Manα1–3 or Manα1–6 linkages, may be recognized as ligand carbohydrates by MBL. Our present finding, an increase in paucimannose oligosaccharides and agalacto forms, might result from an alteration of the biosynthesis pathway of *N*-glycans. The alterations may cause the aberrant glycosylations on most of the glycoproteins rather than some glycoproteins in the SLE-model mouse. The changes in glycosylation might be involved in an autoimmune pathogenesis in the SLE-model mouse kidney.

The continuous production of aberrant antibodies that react with components from self-tissue and accumulation in the immune complex are thought to promote tissue damage in autoimmune disease.[55,56] The mechanism of localized accumulation in the immune complex in some tissues remains unknown in SLE. We found an increase in glycans that may bind to MBL and subsequently promote complement activation via the lectin pathway in the mouse kidney. Our present results suggest that an aberrant *N*-glycan synthesis pathway as well as an abnormal immune system may be involved in the damage caused by glomerular nephritis in the SLE-model mouse.

Acknowledgements

This study was supported in part by a Grant-in-Aid from the Ministry of Health, Labor, and Welfare, and Core Research for the Evolutional Science and Technology Program (CREST), Japan Science and Technology Corp (JST).

References

1 Dwek RA. Glycobiology: toward understanding the function of sugars. *Chem Rev* 1996; **96**:683–720.
2 Helenius A, Aebi M. Intracellular functions of N-linked glycans. *Science* 2001; **291**:2364–9.
3 Zak I, Lewandowska E, Gnyp W. Selectin glycoprotein ligands. *Acta Biochim Pol* 2000; **47**:393–412.
4 Axford JS. Glycosylation and rheumatic disease. *Biochim Biophys Acta* 1999; **1455**:219–29.
5 Feizi T, Gooi HC, Childs RA, Picard JK, Uemura K, Loomes LM, Thorpe SJ, Hounsell EF. Tumour-associated and differentiation antigens on the carbohydrate moieties of mucin-type glycoproteins. *Biochem Soc Trans* 1984; **12**:591–6.
6 Kannagi R, Izawa M, Koike T, Miyazaki K, Kimura N. Carbohydrate-mediated cell adhesion in cancer metastasis and angiogenesis. *Cancer Sci* 2004; **95**:377–84.
7 Goodarzi MT, Turner GA. Decreased branching, increased fucosylation and changed sialylation of alpha-1-proteinase inhibitor in breast and ovarian cancer. *Clin Chim Acta* 1995; **236**:161–71.
8 Yamashita K, Fukushima K, Sakiyama T, Murata F, Kuroki M, Matsuoka Y. Expression of Sia alpha 2→6Gal beta 1→4GlcNAc residues on sugar chains of glycoproteins including carcinoembryonic antigens in human colon adenocarcinoma: applications of *Trichosanthes japonica* agglutinin I for early diagnosis. *Cancer Res* 1995; **55**:1675–9.
9 Tomana M, Schrohenloher RE, Reveille JD, Arnett FC, Koopman WJ. Abnormal galactosylation of serum IgG in patients with systemic lupus erythematosus and members of families with high frequency of autoimmune diseases. *Rheumatol Int* 1992; **12**:191–4.
10 Mizuochi T, Hamako J, Nose M, Titani K. Structural changes in the oligosaccharide chains of IgG in autoimmune MRL/Mp-lpr/lpr mice. *J Immunol* 1990; **145**:1794–8.
11 Arnold JN, Wormald MR, Sim RB, Rudd PM, Dwek RA. The impact of glycosylation on the biological function and structure

of human immunoglobulins. *Annu Rev Immunol* 2007; **25**:21–50.

12 Das H, Atsumi T, Fukushima Y *et al.* Diagnostic value of anti-agalactosyl IgG antibodies in rheumatoid arthritis. *Clin Rheumatol* 2004; **23**:218–22.

13 Raghav SK, Gupta B, Agrawal C, Saroha A, Das RH, Chaturvedi VP, Das HR. Altered expression and glycosylation of plasma proteins in rheumatoid arthritis. *Glycoconj J* 2006; **23**:167–73.

14 Elliott MA, Elliott HG, Gallagher K, McGuire J, Field M, Smith KD. Investigation into the concanavalin A reactivity, fucosylation and oligosaccharide microheterogeneity of alpha 1-acid glycoprotein expressed in the sera of patients with rheumatoid arthritis. *J Chromatogr B Biomed Sci Appl* 1997; **688**:229–37.

15 Rops AL, van den Hoven MJ, Bakker MA *et al.* Expression of glomerular heparan sulphate domains in murine and human lupus nephritis. *Nephrol Dial Transplant* 2007; **22**:1891–902.

16 Chui D, Sellakumar G, Green R *et al.* Genetic remodeling of protein glycosylation *in vivo* induces autoimmune disease. *Proc Natl Acad Sci USA* 2001; **98**:1142–7.

17 Green RS, Stone EL, Tenno M, Lehtonen E, Farquhar MG, Marth JD. Mammalian *N*-glycan branching protects against innate immune self-recognition and inflammation in autoimmune disease pathogenesis. *Immunity* 2007; **27**:308–20.

18 Wada Y. Mass spectrometry in the detection and diagnosis of congenital disorders of glycosylation. *Eur J Mass Spectrom (Chichester, Eng)* 2007; **13**:101–3.

19 Faid V, Chirat F, Seta N, Foulquier F, Morelle W. A rapid mass spectrometric strategy for the characterization of N- and *O*-glycan chains in the diagnosis of defects in glycan biosynthesis. *Proteomics* 2007; **7**:1800–13.

20 Miyamoto S. Clinical applications of glycomic approaches for the detection of cancer and other diseases. *Curr Opin Mol Ther* 2006; **8**:507–13.

21 Yuan J, Hashii N, Kawasaki N, Itoh S, Kawanishi T, Hayakawa T. Isotope tag method for quantitative analysis of carbohydrates by liquid chromatography-mass spectrometry. *J Chromatogr A* 2005; **1067**:145–52.

22 Alvarez-Manilla G, Warren NL, Abney T, Atwood J III, Azadi P, York WS, Pierce M, Orlando R. Tools for glycomics: relative quantitation of glycans by isotopic permethylation using 13CH3I. *Glycobiology* 2007; **17**:677–87.

23 Kang P, Mechref Y, Kyselova Z, Goetz JA, Novotny MV. Comparative glycomic mapping through quantitative permethylation and stable-isotope labeling. *Anal Chem* 2007; **79**:6064–73.

24 Bowman MJ, Zaia J. Tags for the stable isotopic labeling of carbohydrates and quantitative analysis by mass spectrometry. *Anal Chem* 2007; **79**:5777–84.

25 Watanabe-Fukunaga R, Brannan CI, Copeland NG, Jenkins NA, Nagata S. Lymphoproliferation disorder in mice explained by defects in Fas antigen that mediates apoptosis. *Nature* 1992; **356**:314–7.

26 Adachi M, Watanabe-Fukunaga R, Nagata S. Aberrant transcription caused by the insertion of an early transposable element in an intron of the Fas antigen gene of lpr mice. *Proc Natl Acad Sci USA* 1993; **90**:1756–60.

27 Merino R, Iwamoto M, Fossati L, Izui S. Polyclonal B cell activation arises from different mechanisms in lupus-prone (NZB × NZW)F_1 and MRL/Mpl-lpr/lpr mice. *J Immunol* 1993; **151**:6509–16.

28 Homma H, Tozawa K, Yasui T, Itoh Y, Hayashi Y, Kohri K. Abnormal glycosylation of serum IgG in patients with IgA nephropathy. *Clin Exp Nephrol* 2006; **10**:180–5.

29 Hase S, Okawa K, Ikenaka T. Identification of the trimannosylchitobiose structure in sugar moieties of Japanese quail ovomucoid. *J Biochem* 1982; **91**:735–7.

30 Kubelka V, Altmann F, Kornfeld G, Marz L. Structures of the N-linked oligosaccharides of the membrane glycoproteins from three lepidopteran cell lines (Sf-21, IZD-Mb-0503, Bm-N). *Arch Biochem Biophys* 1994; **308**:148–57.

31 Natsuka S, Adachi J, Kawaguchi M, Nakakita S, Hase S, Ichikawa A, Ikura K. Structural analysis of N-linked glycans in *Caenorhabditis elegans*. *J Biochem* 2002; **131**:807–13.

32 Altmann F, Schwihla H, Staudacher E, Glossl J, Marz L. Insect cells contain an unusual, membrane-bound beta-*N*-acetylglucosaminidase probably involved in the processing of protein *N*-glycans. *J Biol Chem* 1995; **270**:17344–9.

33 Guo S, Sato T, Shirane K, Furukawa K. Galactosylation of N-linked oligosaccharides by human beta-1,4-galactosyltransferases I, II, III, IV, V, and VI expressed in Sf-9 cells. *Glycobiology* 2001; **11**:813–20.

34 Jeddi PA, Lund T, Bodman KB *et al.* Reduced galactosyltransferase mRNA levels are associated with the agalactosyl IgG found in arthritis-prone MRL-lpr/lpr strain mice. *Immunology* 1994; **83**:484–8.

35 Cameron JS. Lupus nephritis. *J Am Soc Nephrol* 1999; **10**:413–24.

36 Walport MJ. Complement. First of two parts. *N Engl J Med* 2001; **344**:1058–66.

37 Walport MJ. Complement. Second of two parts. *N Engl J Med* 2001; **344**:1140–4.

38 Botto M. Links between complement deficiency and apoptosis. *Arthritis Res* 2001; **3**:207–10.

39 Hanayama R, Tanaka M, Miyasaka K, Aozasa K, Koike M, Uchiyama Y, Nagata S. Autoimmune disease and impaired uptake of apoptotic cells in MFG-E8-deficient mice. *Science* 2004; **304**:1147–50.

40 Arason GJ, Steinsson K, Kolka R, Vikingsdottir T, D'Ambrogio MS, Valdimarsson H. Patients with systemic lupus erythematosus are deficient in complement-dependent prevention of immune precipitation. *Rheumatology (Oxford)* 2004; **43**:783–9.

41 Cook HT, Botto M. Mechanisms of disease: the complement system and the pathogenesis of systemic lupus erythematosus. *Nat Clin Pract Rheumatol* 2006; **2**:330–7.

42 Gunnarsson I, Sundelin B, Heimburger M, Forslid J, van Vollenhoven R, Lundberg I, Jacobson SH. Repeated renal biopsy in proliferative lupus nephritis – predictive role of serum C1q and albuminuria. *J Rheumatol* 2002; **29**:693–9.

43 Buyon JP, Tamerius J, Belmont HM, Abramson SB. Assessment of disease activity and impending flare in patients with systemic lupus erythematosus. Comparison of the use of complement split products and conventional measurements of complement. *Arthritis Rheum* 1992; **35**:1028–37.

44 Markiewski MM, Lambris JD. The role of complement in inflammatory diseases from behind the scenes into the spotlight. *Am J Pathol* 2007; **171**:715–27.

45 Sturfelt G. The complement system in systemic lupus erythematosus. *Scand J Rheumatol* 2002; **31**:129–32.

46 Holmskov U, Malhotra R, Sim RB, Jensenius JC. Collectins: collagenous C-type lectins of the innate immune defense system. *Immunol Today* 1994; **15**:67–74.

47 Weis WI, Drickamer K, Hendrickson WA. Structure of a C-type mannose-binding protein complexed with an oligosaccharide. *Nature* 1992; **360**:127–34.

48 Takahashi M, Mori S, Shigeta S, Fujita T. Role of MBL-associated serine protease (MASP) on activation of the lectin complement pathway. *Adv Exp Med Biol* 2007; **598**:93–104.

49 Turner MW. Mannose-binding lectin: the pluripotent molecule of the innate immune system. *Immunol Today* 1996; **17**:532–40.

50 Holmskov U, Malhotra R, Sim RB, Jensenius JC. Collectins: collagenous C-type lectins of the innate immune defense system. *Immunol Today* 1994; **15**:67–74.

51 Thiel S, Vorup-Jensen T, Stover CM *et al.* A second serine protease associated with mannan-binding lectin that activates complement. *Nature* 1997; **386**:506–10.

52 Lhotta K, Wurzner R, Konig P. Glomerular deposition of mannose-binding lectin in human glomerulonephritis. *Nephrol Dial Transplant* 1999; **14**:881–6.

53 Ohsawa I, Ohi H, Tamano M *et al.* Cryoprecipitate of patients with cryoglobulinemic glomerulonephritis contains molecules of the lectin complement pathway. *Clin Immunol* 2001; **101**:59–66.

54 Trouw LA, Seelen MA, Duijs JM *et al.* Activation of the lectin pathway in murine lupus nephritis. *Mol Immunol* 2005; **42**:731–40.

55 Jorgensen TN, Gubbels MR, Kotzin BL. New insights into disease pathogenesis from mouse lupus genetics. *Curr Opin Immunol* 2004; **16**:787–93.

56 Lauwerys BR, Wakeland EK. Genetics of lupus nephritis. *Lupus* 2005; **14**:2–12.

J. Biochem. 144, 399–408 (2008)
doi:10.1093/jb/mvn082

Gene Expression Profiling of Human Mesenchymal Stem Cells for Identification of Novel Markers in Early- and Late-Stage Cell Culture

Shihori Tanabe*, Yoji Sato, Takayoshi Suzuki, Kazuhiro Suzuki, Taku Nagao and Teruhide Yamaguchi†

Division of Cellular and Gene Therapy Products, National Institute of Health Sciences, Tokyo 158-8501, Japan

Received January 9, 2008; accepted June 5, 2008; published online June 11, 2008

Human mesenchymal stem cells (hMSCs) are multipotent cells that differentiate into several cell types, and are expected to be a useful tool for cellular therapy. Although the hMSCs differentiate into osteogenic cells during early to middle stages, this differentiation capacity decreases during the late stages of cell culture. To test a hypothesis that there are biomarkers indicating the differentiation potential of hMSCs, we performed microarray analyses and profiled the gene expression in six batches of hMSCs (passages 4–28). At least four genes [necdin homolog (mouse) (*NDN*), EPH receptor A5 (*EPHA5*), nephroblastoma overexpressed gene (*NOV*) and runt-related transcription factor 2 (*RUNX2*)] were identified correlating with the passage numbers in all six batches. The results showed that the osteogenic differentiation capacity of hMSCs is down-regulated in the late stages of cell culture. It seemed that adipogenic differentiation capacity was also down-regulated in late stage of the culture. The cells in late stage are oligopotent and the genes identified in this study have the potential to act as quality-control markers of the osteogenic differentiation capacity of hMSCs.

Key words: cellular therapy, culture stage marker, differentiation, gene expression, stem cell.

Abbreviations: EPHA5, EPH receptor A5; hMSCs, human mesenchymal stem cells; NDN, necdin homolog (mouse); NOV, nephroblastoma overexpressed gene; PBS, phosphate buffered saline; RUNX2, runt-related transcription factor 2.

INTRODUCTION

'Cellular therapy' is a new concept in treating diseases with cells that have regeneration potential. Currently, it is at the clinical research stage; however, the use of cellular therapeutics in regular clinical settings will be implemented in near future. Cellular therapeutics involves the use of cells derived from human tissue, either cultured and/or modified, in regenerating and repairing damaged tissues and consequently improving the functions in the human body. Hence, tissue or embryonic stem cells that have the potential to differentiate into a variety of cell types are one of the prime candidate cells for cellular therapeutics. It is difficult to overview the entire discipline of cellular therapeutics since the cells themselves represent 'life'.

Stem cells, one of the candidates for cellular therapeutics, produce daughter cells identical to themselves that differentiate into other types of cells (*1*). The fate of the stem cells is determined by cellular signaling, although the underlying mechanism is still unknown. It is therefore important to investigate the gene expression patterns that influence the cellular signaling pathways and identify the representative biomarkers that can act as indicators of the differentiation potential of the stem cells. Recently, it has been reported that human somatic cells can be induced to pluripotent stem cells (*2*).

There have been several reports suggesting that cellular therapeutics is a promising treatment for several diseases. C-kit-expressing cells obtained from the bone marrow have been used in cardiac tissue repair in mice experiments (*3*). Previous studies have reported the use of autologous bone marrow cells transplantation for the post-infarction recovery of cardiac function (*4–9*). Cytotoxic T cells have also been used for cellular therapy to protect from infectious diseases in an immunodeficient condition following hematopoietic stem cell transplantation (*10*). Mesenchymal stem cells (MSCs) are also used for therapy expecting immunosuppressive effects (*11*, *12*). Previous studies on MSCs also indicate that these cells possess the ability for chondrogenic (*13*), osteogenic (*14*, *15*) and adipogenic differentiation, and possibly other differentiating capabilities (*16*). In a clinical setting, it is difficult to assess the overall profile of each batch of the cells. We hypothesized the existence of quality-control markers for the differentiation potential of human mesenchymal stem cells (hMSCs) and used gene expression profiling to identify these markers.

*To whom correspondence should be addressed. Tel: +81-3-3700-1141, Fax: +81-3-3700-9217, E-mail: stanabe@nihs.go.jp
†Present address: Division of Biological Chemistry and Biologicals, National Institute of Health Sciences

EXPERIMENTAL PROCEDURES

Cell Culture—The hMSCs derived from bone marrow [Lonza (Cambrex), Walkersville, Maryland, USA] were cultured in mesenchymal stem cell growth medium (MSCGM) [Lonza (Cambrex) #PT-3001; mesenchymal stem cell basal medium supplemented with mesenchymal cell growth supplement, L-glutamine and penicillin/streptomycin] at 37 C in CO_2 (5%) incubator. Cells were passaged according to the manufacturer's protocol with slight modification using trypsin–EDTA solution [Lonza (Cambrex) #CC-3232]. Lot numbers of the hMSC batches were as follows: #4F1127, #4F0312, #5F0138, #4F1560, #4F0591 and #4F0760. Informed consent was obtained in Poietics human mesenchymal stem cell systems [Lonza (Cambrex)]. All differentiation procedures were performed according to Lonza (Cambrex) protocol with slight modification.

Osteogenic Differentiation—The hMSCs were plated onto 12-well plates and 24 h later, the medium was changed to MSCGM (as control) or osteogenic induction medium (OIM) [Lonza (Cambrex) #PT-3002; differentiation basal medium containing dexamethasone, ascorbate, mesenchymal cell growth supplement, L-glutamine, penicillin/streptomycin and β-glycerophosphate]. Medium was changed every 3–4 days and cells were differentiated for 21 days.

Calcium Deposition Assay—Calcium deposition was measured using the Stanbio Total Calcium Liquicolor® kit (Stanbio Laboratory, Boerne, Texas, USA; #0150-250) according to the manufacturer's protocol (Cambrex, Stanbio Laboratory). Briefly, the cells cultured on 12-well plates for 22 days (osteogenic-induced for 21 days) were rinsed with phosphate buffered saline (PBS) without calcium and magnesium [Lonza (Cambrex) #17-516Q] and harvested in 0.5 N HCl (600 µl). Calcium was extracted from the cells by shaking the tubes for approximately 20 h at 4 C. Lysates were centrifuged at 500*g* for 2 min at 4 C and 20 µl of the supernatant was used for the assay. Absorption at 560 nm was measured to detect the Ca-ortho-cresolphthalein complexone (OCPC) complex using an EnVision 2103 multilabel reader (PerkinElmer, Waltham, Massachusetts, USA). Calcium deposition was adjusted with the total protein concentration of the samples. Cells harvested in 0.5 N HCl were centrifuged at 15,000 rpm for 10 min at 4 C. The pellet was washed once with PBS without calcium and magnesium, and resuspended in 100 µl of 0.1 N NaOH/0.1% SDS. After overnight incubation at 37 C, the lysate was centrifuged at 15,000 rpm for 10 min at room temperature, and the supernatant was quantitated using the DC protein assay (Bio-Rad Laboratories, Hercules, California, USA) according to the manufacturer's protocol. Absorbance at 620 nm was measured using the EnVision 2103 multilabel reader (PerkinElmer). The standard curve was obtained using bovine serum albumin.

Adipogenic Differentiation—The cells were plated onto a 24 well-plate at 2.1 x 10^4/cm^2, and cultured in MSCGM for 5–6 days. After cells reach confluence, medium was changed to MSCGM (as control) or adipogenic induction medium (AIM) [Lonza (Cambrex) #PT-3004; induction basal medium supplemented with recombinant human insulin, L-glutamine, mesenchymal stem cell growth supplement, penicillin/streptomycin, dexamethasone, indomethacin and IBMX (3-Isobutyl-1-methylxanthine)]. Medium was changed after 3 days into adipogenic maintenance medium (maintenance basal medium supplemented with recombinant human insulin, L-glutamine, penicillin/streptomycin and mesenchymal stem cell growth supplement). After three complete cycles of induction/maintenance, the cells were cultured for 7 more days in adipogenic maintenance medium, replacing the medium every 2–3 days.

Oil Red O staining—The cells were rinsed with 500 µl of PBS and fixed with 10% neutral buffered formalin (500 µl). After washing with sterile water, the cells were washed with 60% 2-propanol (500 µl) for 2–5 min and stained with Oil Red O (500 µl) for 5 min. The cells were rinsed with tap water and stained with Harris' haematoxylin (500 µl) for 1 min and rinsed with the water. Lipid vesicles were observed with microscope Biozero BZ-8000 (KEYENCE, Osaka, Japan).

Chondrogenic Differentiation—The cells (3×10^5) were washed with incomplete chondrogenic induction medium [Lonza (Cambrex) #PT-3003; chondrogenic basal medium containing dexamethasone, ascorbate, ITS (insulin-transferrin-sodium selenite) + supplement, sodium pyruvate, proline, penicillin/streptomycin, L-glutamine] and were resuspended in 0.5 ml of complete chondrogenic induction medium (CCIM; incomplete condrogenic induction medium supplemented with 10 ng/ml of TGF-β3) or MSCGM (as control) and cultured in 15 ml polypropylene culture tubes. The medium was replaced every 3–4 days and the cells were cultured for 24 days.

Safranin-O Stains for in vitro Chondrogenesis—The chondrogenic pellets were fixed in 10% neutral buffered formalin and paraffin embedded. The paraffin sections were stained with Weigert's iron hematoxylin (Wako 298-21741), 0.02% fast green FCF (MP biomedicals 195178) and 0.1% Safranin-O (Sigma HT 90432), followed by observation with microscope Biozero BZ-8000 (KEYENCE).

Total RNA Purification—The hMSCs were cultured on a 10 cm dish, lysed in 600 µl of Buffer RLT (RNeasy® Lysis Buffer) with β-mercaptoethanol and homogenized using a QIA shredder (QIAGEN, Düsseldorf, Germany). Total RNA was purified using RNeasy® mini spin columns according to manufacturer's protocol (QIAGEN). Total RNA was eluted with RNase-free water.

Microarray Analysis—Total RNA (100 ng or 1 µg) was reverse transcribed and amplified using a GeneChip® kit (Affymetrix, Santa Clara, California, USA) and the biotinylated cRNA was hybridized onto the GeneChip® Human Genome U133 Plus 2.0 Array (54,613 probe sets). The data was analysed using GeneChip Operating System software (versions 1.2–1.4), followed by statistical analysis. The data was also analysed using GeneSpring™ (version 7.3) (Agilent, Santa Clara, California, USA). The data discussed in this publication have been deposited in NCBI's Gene Expression Omnibus (GEO; http://www.ncbi.nlm.nih.gov/geo/) (*17*, *18*). They are accessible through GEO Series accession number GSE7637 for the data from 4F1560, and GSE7888 for the data obtained from all six batches. The statistical method for microarray data analysis has been also discussed elsewhere (*19*).

Cluster Analysis—The microarray data of 169 probe sets obtained from six batches of hMSCs was subject to cluster analysis using the Gene Expression Statistical System (NCSS, Kaysville, Utah; Dr Jerry L. Hintze). Fold change of signal intensity to the average signal intensity of early stage was analysed and a double dendrogram was plotted on a log 2 scale.

Gene Ontology Analysis—Gene ontology analysis was conducted using Ingenuity Pathway Analysis (IPA) (Ingenuity® Systems, Redwood City, California, USA), NetAffyx (Affymetrix) and GOTM (Gene Ontology Tree Machine, Vanderbilt University, Nashville, Tennessee, USA) analyses. Probe sets with signal intensity values associated with the passage numbers were subject to analyses. The functional analysis identified the biological function and/or diseases that were most significant to the data set. Genes from the data set that were associated with biological functions and/or diseases in the Ingenuity Pathways Knowledge Base (IPKB) were considered for further analysis.

cDNA Synthesis and Real-time PCR Using Taqman Low-density Array—RT–PCR (reverse transcriptase–PCR) analysis was performed to assess the mRNA levels in six batches of hMSCs using TaqMan® low-density array (TLDA) (Format 48) (Applied Biosystems, Foster City, California, USA). The data was normalized using *GAPDH* (glyceraldehyde-3-phosphate dehydrogenase). Forty-six genes including *GAPDH* as endogenous control are listed in Supplementary Table 1. cDNA was synthesized using a High-capacity cDNA synthesis kit (Applied Biosystems) and Multiscribe reverse transcriptase. cDNA synthesized from 100 ng of total RNA was used for the analysis (2 ng of total RNA per well). Real-time PCR was analysed using 7900 HT real-time PCR system (Applied Biosystems). The conditions for the PCR reaction were as follows: 50°C (2 min) and 94.5°C (10 min), and 40 cycles at 97°C (30 sec) and 59.7°C (1 min). Relative quantification values were calculated by the comparative Ct method using SDS 2.2.2 software (Applied Biosystems).

Pathway Network Analysis—Data were analysed using the IPA (Ingenuity® Systems, www.ingenuity.com). A data set containing gene identifiers and corresponding expression values was uploaded into the application. Each gene identifier was mapped to its corresponding gene object in the IPKB. A fold-change cutoff of 3 for both up- and down-regulation and a p-value cutoff of 0.05 were set to identify the genes to be analysed. These genes, called focus molecules, were overlaid onto a global molecular network developed from information in the IPKB. Networks of these focus molecules were then algorithmically generated based on their connectivity. The functional analysis of a network identified the biological functions and/or diseases that were most significant to the genes in the network. The genes in the networks associated with biological functions and/or diseases in the IPKB were considered for the analysis. Genes and gene products are represented as nodes, and the biological relationship between two nodes is represented as an edge (line). All edges are supported by at least one reference from the literature, textbook or canonical information stored in the IPKB. Human, mouse and rat orthologs of a gene are stored as separate objects in the IPKB, but are represented as a single node in the network. The node colour indicates the degree of up- (red) or down- (green) regulation. Nodes are displayed using various shapes that represent the functional class of the gene product.

Statistical Analyses—Non-parametric analysis was used for microarray data analyses. The Spearman correlation coefficient and two-tailed p-values were calculated. $P < 0.001$ or $P < 0.05$ were considered to be significant. RT–PCR data was analysed with non-parametric analysis. The Spearman correlation coefficient and two-tailed p-values were calculated. To compare the specific passage number and stage, Student's t test was performed. Two-way ANOVA followed by Bonferroni post-test was performed for osteogenesis data. GraphPad Prism® 4 and Microsoft® Office Excel were used for statistical analysis and drawing graphs.

RESULTS

Microarray Analysis of hMSCs—To identify the quality-control markers in different stage of the culture, we performed DNA microarray analyses. Non-parametric analysis and a ratio (max/min of signal intensity) cutoff of 3.071,524 ($1.05^{[28-5]}$; 5% change in each passage from 5th to 28th) showed that the expression level of 341 probe sets out of a total of 54,613 probe sets had a significant association with passage numbers (hMSC lot #4F1560, passage numbers 5, 7, 9, 13, 21 and 28).

Gene ontology analyses showed that the mapped genes corresponded to the probe sets belonging to various categories of molecular and cellular functions such as cell-to-cell signaling and interaction, cellular movement, cell death, cellular assembly, cellular organization and cell cycle, and physiological system development, and biological functions such as hematological system development and function, immune and lymphatic system development and function, tissue development, immune response and embryonic development. The top five disease categories that the genes mapped to, as identified using the IPA software, included cardiovascular, hematological, musculoskeletal, oncogenic and reproductive disorders.

Figure 1 shows the results of cluster analysis obtained from microarray data of six batches of hMSCs in early (passage #4–5), middle (#7–9) and late stages (#22–28). Seventy-nine genes out of the 169 probe sets were categorized by function and disease as per IPA analysis. Networks were analysed for each of the six batches and a representative network is shown in the Supplementary Fig. 1. A list of all top networks in each analysis is shown in Table 1. Many network categories with the top score in each analysis were involved in cancer or regulation of cell cycle. Additionally, specific networks for each sample were generated when the batches were individually analysed.

Calcium Deposition of Osteogenic-induced Cells—In Fig. 2, calcium deposition in hMSC cultures (4F0312, 5F0138, 4F1560, 4F0591, 4F0760) were measured during passages 7, 9, 10 and 19. The results showed that the osteogenic differentiation occurred in early to middle stages and was dramatically suppressed during the late

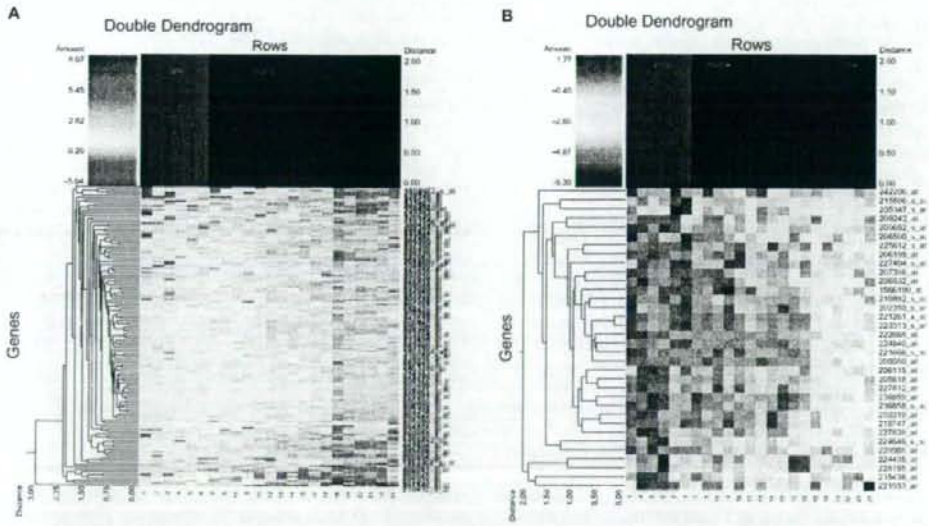

Fig. 1. **Microarray analysis of hMSCs.** One hundred and sixty-nine probe sets extracted from microarray data of six batches of hMSCs. [$n = 6$ in early stage (#4 or 5), passage #9, late stage (#22, 24 or 28), $n = 5$ in passage #7]. Cut off value of signal intensity ratio (max/min of average in each stage) is 2.949145023 [5% change in each passage number from early to late stage; 1.05 (passage number range of average in early and late stage)]. Double dendrograms of up-regulated 135 probe sets (A) and down-regulated 34 probe sets (B) are shown.

stages of cell culture. These findings suggest that the expression levels of genes associated with osteogenesis are different at the late stages compared with those at earlier stages of cell culture.

Statistical analysis of microarray and calcium deposition data from three batches (5F0138, 4F1560, 4F0591) of hMSCs in middle (#7–10) and late (#19–28) stages showed that the expression of *NDN* [necdin homolog (mouse)] has a positive correlation with calcium deposition ($P < 0.05$).

Adipogenic Differentiation of hMSCs—Figure 3A shows the results of Oil Red O staining of adipogenic-induced cells. The cells were adipogenic induced for 21 days and lipid was stained with Oil Red O. Adipogenesis of hMSCs seemed to be down-regulated in late culture stage of 5F0138, 4F0591 and 4F0760, while the adipogenic-differentiation capacity seemed to be retained in passage #20 of 4F1560.

Chondrogenic Differentiaion of hMSCs—Figure 3B shows the Safranin-O staining of chondrogeninc-differentiated hMSCs. The cells were differentiated in CCIM for 24 days and stained with Safranin-O. The culture in passages 7, 17 and 22 of 4F0591 showed chondrogenic-differentiated morphology (a, b, c, respectively). The culture in late stage seemed to be chondrogenic differentiated as shown (c). The cells cultured in MSCGM as control did not show any chondrogenic-differentiated morphology (d).

RT-PCR Analysis of hMSCs—The quantitative RT-PCR data showed that some genes had similar expression profiles in all the six batches examined. Up-regulated genes, which were identified as candidates for the stage-specific markers included *EPHA5* (EPH receptor A5), *NOV* (nephroblastoma overexpressed gene), *SERPINE1* [serpin peptidase inhibitor clade E (nexin, plasminogen activator inhibitor type 1), member 1], *ITGA4* [integrin, alpha 4 (antigen CD49D, alpha 4 subunit of VLA-4 receptor)], and down-regulated genes, which are also candidates for the stage-specific markers included *NDN*, *RUNX2* (runt-related transcription factor 2) and *RUNX3* (runt-related transcription factor 3). *NOV* is a growth factor and is involved in the proliferation of bone cancer cell lines (*20*). It is notable that the expression of *NOV* in lot #4F1127 was relatively stable. *SERPINE1* is involved in the protein-binding function and diseases such as heart failure (*21*). *RUNX2* is a member of the runt domain-containing family of transcription factors and suggested to regulate osteogenic differentiation (*22*). *RUNX3* is also a member of the runt domain-containing family of transcription factors and a candidate tumor suppressor (*23*). *EPHA5*, *NOV*, *NDN* and *RUNX2* showed altered expression correlating with passage numbers ($P < 0.01$) (Fig. 4). The results of RT–PCR analysis of 45 genes examined are shown in Supplementary Fig. 2.

DISCUSSION

hMSCs will be used for cellular therapeutics in clinical settings in the near future. The importance of quality control of the cells will be significant as the use of cellular therapeutics becomes more common. In this report, we report on profiling the gene expression of

Table 1. **List of the networks in hMSCs.**

Analysis	Molecules in network	Score	Focus molecules	Top functions
4F0591-#9	BUB1B, CCNB1, CDC2, CDKN3, CENPF, CGREF1, Cyclin E, DLG7, E2f, ERCC6L, FOXM1, KRT8, LRP1, MAD2L1, MEOX2, NDC80, NFkB, NUF2, NUSAP1, OLR1, PBK, PCSK1, PLK1, PTTG1, RAD51AP1, Rb, RNA polymerase II, RRM2, SERPINB2, SPC25, TFPI2, TNFSF9, TRADD, TYMS, UBE2C	65	30	Cell Cycle, Cancer, Reproductive System Disease
4F1560-#28	ADH1B, ALDH1A3, BEX1 (includes EG:55859), BMP15, CD80, CHI3L1, DBP, DLX1, ENPP1, FGF5, GBP2, IGF2, Igfbp, IGFBP5, KRT19, LBP, MEOX2, Mmp, NFkB, NOV, PCSK1, PCSK5, PEG10, PYCARD, RAGE, SEPP1, SERPINB2, SERPING1, ST8SIA1, Tgf beta, TLR1, TNFAIP6, TNFSF15, TRAF4, TSLP	57	31	Cancer, Cellular Growth and Proliferation, Neurological Disease
4F0760-#9	ANKRD1, Ap1, BIRC3, CCNB1, CCR2, CDC2, CENPE, COL15A1, FBLN5, Jnk, LATS1, Mmp, MSR1, NDC80, NFkB, NRL, NUF2, OMD, PBK, Pdgf, PDGF BB, PDGFD, PRDM1, S100A4, SERPINB2, SLC37A4, SORBS3, SPC24, SPC25, TFPI2, THBD, TNFRSF8, VANGL2, VAV3, VSNL1	56	29	Cancer, Cell Cycle, Reproductive System Disease
5F0138-#24	ARL4C, BUB1 (includes EG:699), BUB1B, CCNB1, CCNB2, CCNF, CDC2, CDC7, CDC20, CDC25C, CDKN3, CENPE, CENPH, Cyclin B, Cyclin E, FBXO5, FOXM1, GINS1, GPNMB, IL6, KIAA0101, KIF11, KIF22, KIF2C, MRVI1, NDC80, NUF2, PBK, PLK4, PTTG1, SLC7A7, SPC25, UBE2C, VTCN1, ZWINT (includes EG:11130)	52	33	Cell Cycle, Cancer, DNA Replication, Recombination, and Repair
4F1560-#9	14-3-3, AURKA, BIRC5, CCNB1, CDC20, CDC25C, CDCA8, Cyclin B, Cyclin E, E2f, IGF2, MAD2L1, NDC80, NFkB, NUF2, OLR1, PBK, PRR11, RAD51AP1, Rb, RGS7, RNA polymerase II, RRM2, Scf, SERPINB2, SFN, SFRP4, SPC24, SPC25, TNFRSF8, TOP2A, TYMS, UBE2C, UHRF1, ZNF74	52	27	Cancer, Cell Cycle, Reproductive System Disease
4F0591-#28	AEBP1, ALDH1A3, ANGPT1, ANKRD1, BEX1 (includes EG:55859), C1R, CGREF1, CXCL16, DIRAS3, GAD1, HDAC9, ID4, IL1, IL1R1, KRT18, KRT19, MEOX2, Mmp, MYBL1, MYPN, NFkB, OLR1, PAK1IP1, Pdgf Ab, PLAT, PYCARD, RIPK4, SERPINB2, SERPINF1, SERPING1, TFPI2, Tgf beta, TNFRSF19, TNFRSF11B, TSLP	51	30	Cancer, Cardiovascular Disease, Cell Death
4F0312-#7	A2M, ACAN, ASPN, BRCA1, C1R, C1S, CEBPD, CYP27A1, DDIT3, DDIT4, ESR1, FGF7, GDF15, IL1, Jnk, KSR2, MAD2L1, Mek, Mek1/2, Mmp, NFkB, NOTCH3, NOX4, NR4A1, OSMR, P38 MAPK, PCK2, Pdgf, PDGF BB, SERPINB2, STAT, TNFAIP6, TNFSF9, TNFSF15, TRIB3	50	25	Cell Cycle, Inflammatory Disease, Cellular Development
4F0312-#28	ANKRD1, BEX1 (includes EG:55859), BLK, CD36, CDKN2B, CTSL2, ENPP1, F2RL1, FABP5, FKBP5, FUS, G0S2, GAD1, GDF15, IGFBP5, IGHG1, IL1, N-cor, NFkB, OLR1, PAPPA2, PLAT, PNRC1, Rxr, RXRA, SERPINB2, STMN2, Tgf beta, THRB, Thyroid hormone receptor, TNFRSF19, TNFRSF11B, TNFSF13B, TRIP13, VSNL1	50	29	Cancer, Cellular Growth and Proliferation, Immunological Disease
4F1560-#7	14-3-3, AURKA, BIRC5, CCNE2 (includes EG:9134), CDC25A, CDCA8, CEBPA, CENPF, CSPG4, Cyclin A, Cyclin E, E2f, ESPL1, FEN1, FMOD, Histone h3, Mapk, MCM8, MCM10, MDM4, NUSAP1, OIP5, PP2A, PRR11, PTTG1, Rb, RGS7, RRM2, SFRP4, SMPDL3A, SOS2, TOP2A, TTK, TYMS, UBE2C	50	27	Cell Cycle, Cancer, Reproductive System Disease
4F0312-#9	ABCA1, ACAN, AEBP1, Akt, ANXA11, ASPN, C1R, C1S, CD36, DKK, F2RL1, FBLN1, FGF7, FOXE1, GDA, GDF15, HSD11B1, IGF2, IGFBP2, Insulin, LDL, LEPR, Mapk, NFkB, NTF3, P38 MAPK, PDGF BB, PTX3, SLC7A7, THBS2, TNFAIP6, TNFSF9, Wnt, WNT2, WNT16	49	23	Lipid Metabolism, Molecular Transport, Small Molecule Biochemistry

(continued)

Table 1. **Continued.**

Analysis	Molecules in network	Score	Focus molecules	Top functions
5F0138-#9	ABCA1, AEBP1, ARG2, BGN, C1q, C1R, C1S, CYP2B6 (includes EG:1555), DDIT4, ENPP1, FABP5, FADS1, GDF15, HABP2, N-cor, NCOR-LXR-Oxysterol-RXR-9 cis RA, NFkB, Nr1h, OLR1, PCK2, PDGF BB, PTGDR, Rxr, SCD, SERPING1, SFTPD, SORBS3, SREBF1, SYNE1, THBS2, Thyroid hormone receptor, TNFAIP6, TNFSF9, TRIB3, VDR	46	27	Respiratory Disease, Inflammatory Disease, Lipid Metabolism
4F1127-#9	ACAN, Alkaline Phosphatase, Ap1, ASPN, C3, CCL2, CCNO, COL13A1, CP, FABP5, GEM, HMOX1, HOMER2, IGFBP5, IL1, JAG1, LDB3, LDL, Mmp, MMP28, NFkB, P38 MAPK, Pdgf, PDGF BB, RGS4, SERPINB2, SPINT2, SPP1, TAC1, Tgf beta, TNFAIP6, TNFRSF11B, TXNIP, VitaminD3-VDR-RXR, ZNF335	45	24	Cellular Development, Cellular Growth and Proliferation, Skeletal and Muscular System Development and Function
4F1127-#22	AEBP1, ANKRD1, C1q, C1R, CBR3, CD36, CFH, ENPP1, FLNC, FOXF1, G0S2, HAMP, HDL, HIST2H2AA3, HIST2H2BE, HIVEP1, IGKC, KCNAB1, KCND2, KRT17, LDB3, LY6E (includes EG:4061), MYOZ1, NFkB, OLR1, PLK3, POU2F2, REG3A, RIPK4, SLC40A1, TNFRSF19, TNFRSF10D, TNFSF9, TSLP, VSNL1	44	32	Genetic Disorder, Metabolic Disease, Molecular Transport
4F0760-#28	Alpha Actinin, CDH1, CTSH, Cyclin A, Cyclin E, E2f, EDN1, GAST, ICAM2, Integrin, ITGA2, ITGA6, KRT7, KRT18, LAMC2, MARCKSL1, Mek1/2, Mmp, MYOZ2, OCLN, PCOLCE, PCOLCE2, Plc beta, PLCB4, PRPS1, Rb, S100A4, SCG5, SDPR, SERPINB2, SMURF2, TFPI2, TGFB1, TNFRSF11B, TSPAN8	44	26	Cardiovascular System Development and Function, Cell Morphology, Skeletal and Muscular System Development and Function
4F0591-#7	AMELX, AQP4, ARNT2, BAT3, beta-estradiol, BIRC5, CATSPERB, CDCA8, CEBPA, CGREF1, DLGAP1, GLIPR1, GPR37, GRIN1, GTSE1, HSPA2, HSPA5, INS1, LITAF, NCAPG (includes EG:64151), NFkB, NPAS1, PLGLB2, RAB31, RAGE, retinoic acid, RPS14, RPS4X, RRM2, SCG2, STXBP4, TF, TGFB1, TP53, TRHDE	38	16	Cell Death, Cancer, Respiratory Disease
4F1127-#7	Actin, ADIPOQ, Akt, Ap1, BCL9, BIRC5, CCL2, CPE, EGR2, ERCC6L, HIST1H4C, Histone h3, HOMER2, IL1, IL8, Jnk, KRT18, LDL, NFkB, OSBP, P38 MAPK, PBK, PDGF BB, PDGFC, PLK1, POSTN, PRDX4, SERPINA3, SFRP4, SLC2A3, Tgf beta, TIFA, TNFRSF11B, TNFRSF1B, TPT1	35	17	Cellular Growth and Proliferation, Cellular Development, Hematological System Development and Function
5F0138-#7	Akt, Ap1, ASNS, CALM2, DAD1, DDIT4, FSTL1, G0S2, GARS, GDF15, HTRA1, JAK3, LDHA, LDL, LOX, MMP1 (includes EG:4312), NFkB, P38 MAPK, PCK2, PCOLCE, PDGF BB, PDGFC, PDPN, RND3, RPN2, SFRP1, SLC7A1, TCR, TGFB1, TIMP4, TNFRSF8, TNFSF9, TRIB3, UGDH, WNT2	30	15	Cancer, Cellular Movement, Cellular Development

The top networks in each analysis data analyzed by IPA are listed.

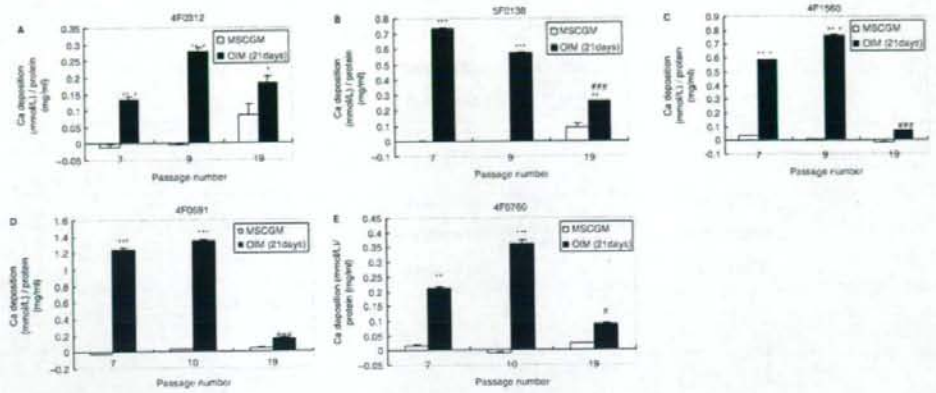

Fig. 2. **Calcium deposition of hMSCs.** The cells in each passage numbers indicated were plated on 12-well plates and cultured in MSCGM (control; clear column) or OIM (osteogenic differentiated; filled column) for 21 days. The amounts of calcium deposition in 4F0312, 5F0138, 4F1560, 4F0591 and 4F0760 are indicated in (A, B, C, D and E), respectively. Calcium deposition divided by protein concentration is showed as mean + SEM in triplicate. $^{***}P<0.001$, $^{**}P<0.01$, $^{*}P<0.05$ when osteogenesis in MSCGM was compared to that in OIM in each passage number. ### $P<0.001$, ## $P<0.01$, # $P<0.05$ when osteogenesis in passage #19 was compared to that in passage number 7 ($n=3$).

hMSCs through early and late stages of cell culture. Replication was performed by testing six different batches of cells. All six batches examined showed a marked decrease in culture growth rate with increasing passages.

The hMSC potential for osteogenic differentiation was down-regulated in all the batches of hMSCs examined during the late culture stage. The osteogenic differentiation was observed in all the batches of hMSCs examined for passages 7, 9 and 10. Also, every batch examined showed a down-regulation of the osteogeneic process during the 19th passage. As previously stated, four genes, *NDN*, *EPHA5*, *NOV* and *RUNX2* showed altered expression depending on the culture stage. *EPHA5* and *NOV* were up-regulated as the cells were further passaged, while *NDN* and *RUNX2* were down-regulated.

RT–PCR data indicated that the expression of *NDN* in all batches examined decreased during the late stages of culture. The expression of *NDN* in lot #4F1127, #4F0312 and #5F0138 was relatively stable until the 14th passage, which was then followed by a decrease in expression during the late stages. Microarray data also showed that the expression of *NDN* in passages 22–28 were decreased compared to that in passages 4–8. Furthermore, our results showed a positive correlation between the expression of *NDN* in hMSCs and the potential to differentiate into osteogenic cells as measured by the calcium deposition rates. Previous reports suggested that necdin, an *NDN* homolog, interacts with IL-1α precursor (*24*). The expression of *NDN* in hMSCs decreases with increasing passages. It is possible that *NDN* down-regulation is involved in activation of IL1-Myd88 pathway by dying cells (*25*).

Every batch showed a passage-dependent increase in the expression level of *EPHA5*. EPHA5 is transmembrane receptor protein tyrosine kinase, known as Ephrin A5 receptor, and belongs to the ephrin receptor subfamily. Recently, it has been shown that EPHA5 is involved in cellular growth and tumor malignancies (*26*, *27*). Also, it is known that the expression level of human *EPHA5* mRNA is high in primary human breast carcinoma cells (*28*).

NOV/CCN3 is a growth factor that plays several roles in cellular migration, growth, proliferation and chemotaxis. The previous finding that *NOV* inhibits the proliferation of a cancer cell line is consistent with the observation that *NOV* expression level is increased in the senescing phase, which coincides with the low proliferative stage of hMSCs. Furthermore, in primary skin fibroblasts, NOV/CCN3 protein increases the expression of human *SERPINE1* mRNA level (*29*). This is consistent with our observation that the expressions of *SERPINE1* as well as *NOV* are up-regulated during the late stages of cell culture. Mutant human SERPINE1 (T333R; A355R), which lacks the protease-inhibitory activity, decreases the quantity of rat laminin and inhibits matrix accumulation (*30*). On the other hand, previous finding indicated that the expression of mouse *Myod1* (myogenic differentiation 1) mRNA level and Myog (myogenin) protein decreased in C2/4 cells (subclone of C2C12 mesenchymal cells) stably expressing NOV, which suggests that NOV suppresses the myogenic differentiation of C2/4 cells (*31*).

The expression of *RUNX2* was also decreased in late stage of the culture. *RUNX2* is a member of the runt family of transcription factors and suggested to be involved in osteogenesis (*22*). It is possible that down-regulated osteogenic differentiation of hMSCs is caused by the decreased expression of *RUNX2*. Recent reports have shown that 3D cultures of human adipose tissue-derived endothelial and osteoblastic progenitors generate osteogenic–vasculogenic constructs (*32*). It might be

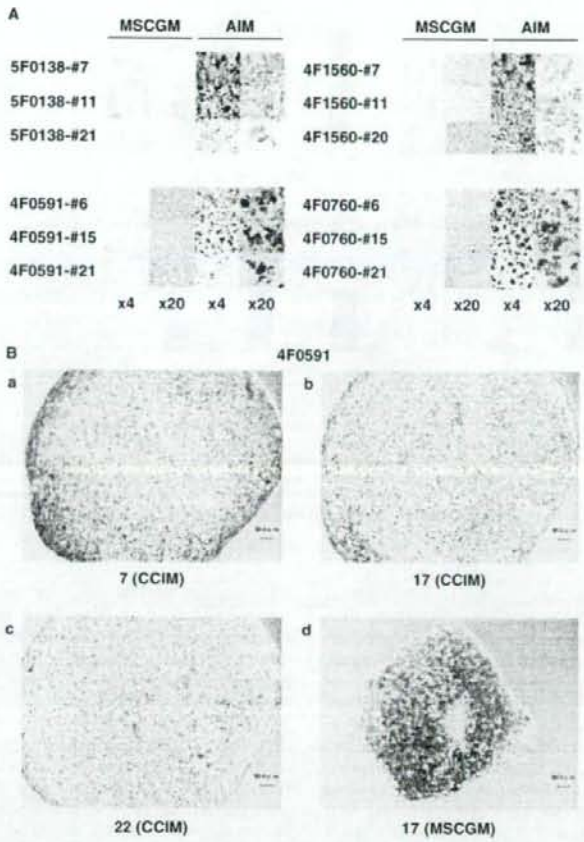

Fig. 3. **Adipogenic differentiation and chondrogenic differentiation of hMSCs.** (A) The cells in each passage numbers indicated were plated on 24-well plates and cultured in MSCGM (as control) or AIM (adipogenic differentiation medium) for 21 days. The cells were stained with Oil Red O. (B) The cells in passage. #7, #17 or #22 of 4F0591 were cultured in CCIM for 24 days and stained with Safranin O (a, b, c, respectively). Proteoglicans stained red. The cells in passage #17 were also cultured in MSCGM (as control) for 24 days (d).

interesting to investigate the gene expression profile of the 3D culture of hMSCs.

In conclusion, microarray and RT–PCR data of the six batches of hMSCs suggested that four genes, *EPHA5*, *NOV*, *NDN* and *RUNX2* have the potential to act as stage-specific markers during hMSC culture. These genes can be used as candidates for quality control markers of the culture status with regard to the differentiation potential for future clinical application of hMSCs for cellular therapeutics. We reported that the capacity of hMSCs for osteogenic differentiation was highly suppressed during the late culture stages. *NDN* or *RUNX2* may be a quality control marker of hMSC capacity for osteogenic differentiation. The observations of adipogenic differentiation of hMSCs suggested that each batch shows different transition in differentiation potential. It seemed that the capacity tends to be suppressed in late stage of the culture. The observations of chondrogenic differentiation suggested that the differentiation potential of hMSCs is retained in late stage of the culture. It seems that the cells in the late stage have limited differentiation potential (oligopotent). Furthermore, network analysis and gene expression analysis revealed that the expression profiles are distinct for each passage number. These findings imply the importance of quality control for safe application of hMSCs for cellular therapy and usefulness of expression analysis for finding marker genes. Phenotype profiling and profiling at the genome level, including chromosomal analysis, might need more research in the future. The profiling of the cells, in both differentiated and 3D states, will also need to be investigated for future clinical applications.

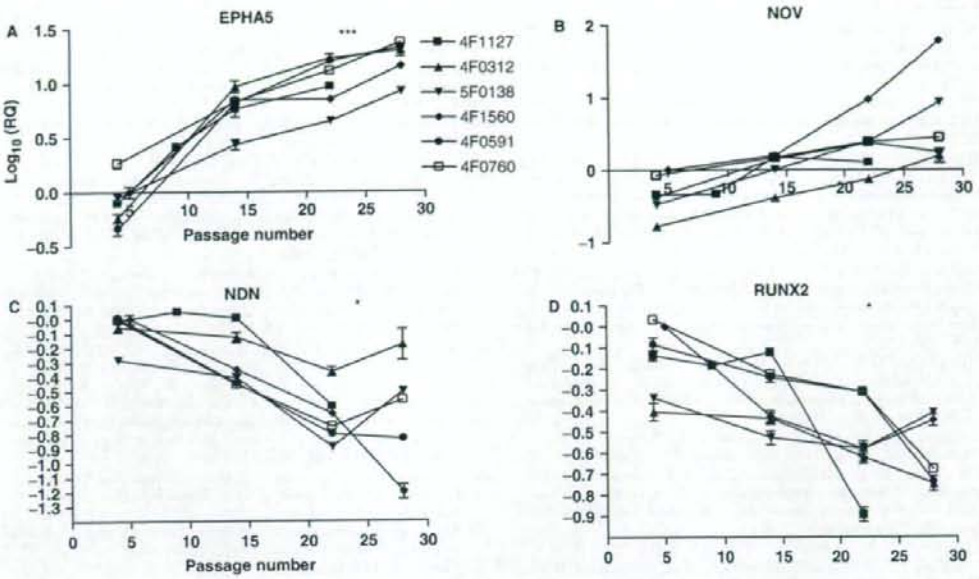

Fig. 4. **Gene expression profiles of culture stage markers suggested for hMSCs.** Individual plots for six batches of hMSCs obtained from RT–PCR data. The expression of *EPHA5* (A), and *NOV* (B) increased, while that of *NDN* (C) and *RUNX2* (D) decreased as the cells were further passaged in each batch. Relative quantity value was plotted on a log 10 scale. The expression of four genes (A–D) was correlated with passage numbers ($P < 0.01$). *** $P < 0.001$, * $P < 0.05$ when the expression in passage #14 was compared to that in late stage (passage #22 and #28) ($n = 6$ in passage #14, $n = 10$ in late stage).

Supplementary data are available at *JB* online.

We thank Dr Y. Hayashi for advice in microarray statistics analysis, and Dr Y. Shinozaki for assistance in microarray experiments. We are also thankful to Dr Y. Ohno and Dr E. Uchida for their support and valuable comments. We are most grateful to C. Aoyagi for her excellent skill in making paraffin sections. This work was supported in part by grants and the Grant-in-Aid for Cancer Research from the Ministry of Health, Labour and Welfare.

REFERENCES

1. Clevers, H. (2005) Stem cells, asymmetric division and cancer. *Nat. Genet.* **37**, 1027–1028
2. Takahashi, K., Tanabe, T., Ohnuki, M., Narita, M., Ichisaka, T., Tomoda, K., and Yamanaka, S. (2007) Induction of pluripotent stem cells from adult human fibroblasts by defined factors. *Cell* **131**, 861–872
3. Fazel, S., Cimini, M., Chen, L., Li, S., Angoulvant, D., Fedak, P., Verma, S., Weisel, R.D., Keating, A., and Li, R.K. (2006) Cardioprotective c-kit+ cells are from the bone marrow and regulate the myocardial balance of angiogenic cytokines. *J. Clin. Invest.* **116**, 1885–1877
4. Rosenzweig, A. (2006) Cardiac cell therapy-mixed results from mixed cells. *N. Engl. J. Med.* **355**, 1274–1277
5. Wollert, K.C., Meyer, G.P., Lotz, J., Lichtenberg, S.R., Lippolt, P., Breidenbach, C., Fichtner, S., Korte, T., Hornig, B., Messinger, D., Arseniev, L., Hertenstein, B., Ganser, A., and Drexler, H. (2004) Intracoronary autologous bone-marrow cell transfer after myocardial infarction: the BOOST randomised controlled clinical trial. *Lancet* **364**, 141–148
6. Schächinger, V., Erbs, S., Elsässer, A., Haberbosch, W., Hambrecht, R., Hölschermann, H., Yu, J., Corti, R., Mathey, D.G., Hamm, C.W., Suselbeck, T., Assmus, B., Tonn, T., Dimmeler, S., and Zeiher, A.M. (2006) Intracoronary bone marrow-derived progenitor cells in acute myocardial infarction. *N. Engl. J. Med.* **355**, 1210–1221
7. Assmus, B., Honold, J., Schächinger, V., Britten, M.B., Fischer-Rasokat, U., Lehmann, R., Teupe, C., Pistorius, K., Martin, H., Abolmaali, N.D., Tonn, T., Dimmeler, S., and Zeiher, A.M. (2006) Transcoronary transplantation of progenitor cells after myocardial infarction. *N. Engl. J. Med.* **355**, 1222–1232
8. Lunde, K., Solheim, S., Aakhus, S., Arnesen, H., Abdelnoor, M., Egeland, T., Endresen, K., Ilebekk, A., Mangschau, A., Fjeld, J.G., Smith, H.J., Taraldsrud, E., Grøgaard, H.K., Bjørnerheim, R., Brekke, M., Müller, C., Hopp, E., Ragnarsson, A., Brinchmann, J.E., and Forfang, K. (2006) Intracoronary injection of mononuclear bone marrow cells in acute myocardial infarction. *N. Engl. J. Med.* **355**, 1199–1209
9. Janssens, S., Dubois, C., Bogaert, J., Theunissen, K., Deroose, C., Desmet, W., Kalantzi, M., Herbots, L., Sinnaeve, P., Dens, J., Maertens, J., Rademakers, F., Dymarkowske, S., Gheysens, O., Cleemput, J.V., Bormans, G., Nuyts, J., Belmans, A., Mortelmans, L., Boogaerts, M., and Van de Werf, F. (2006) Autologous bone marrow-derived stem-cell transfer in patients with ST-segment elevation myocardial infarction: double-blind, randomised controlled trial. *Lancet* **367**, 113–121

10. Peggs, K.S., Verfuerth, S., Pizzey, A., Khan, N., Guiver, M., Moss, P.A., and Mackinnon, S. Adoptive cellular therapy for early cytomegalovirus infection after allogeneic stem-cell transplantation with virus-specific T-cell lines. *Lancet* **362**, 1375–1377
11. Dazzi, F., van Laar, J.M., Cope, A., and Tyndall, A. (2007) Cell therapy for autoimmune diseases. *Arthritis Res. Ther.* **9**, 206–214
12. Ringdén, O., Uzunel, M., Rasmusson, I., Remberger, M., Sundberg, B., Lönnies, H., Marschall, H.-U., Dlugosz, A., Szakos, A., Hassan, Z., Omazic, B., Aschan, J., Barkholt, L., and Le Blanc, K. (2006) Mesenchymal stem cells for treatment of therapy-resistant graft-versus-host disease. *Transplantation* **81**, 1390–1397
13. Derfoul, A., Perkins, G.L., Hall, D.J., and Tuan, R.S. (2006) Glucocorticoids promote chondrogenic differentiation of adult human mesenchymal stem cells by enhancing expression of cartilage extracellular matrix genes. *Stem Cells* **24**, 1487–1495
14. Nuttelman, C.R., Tripodi, M.C., and Anseth, K.S. (2004) *In vitro* osteogenic differentiation of human mesenchymal stem cells photoencapsulated in PEG hydrogels. *J. Biomed. Mater. Res. A* **68**, 773–782
15. Kulterer, B., Friedl, G., Jandrositz, A., Sanchez-Cabo, F., Prokesch, A., Paar, C., Scheideler, M., Windhager, R., Preisegger, K.-H., and Trajanoski, Z. (2007) Gene expression profiling of human mesenchymal stem cells derived from bone marrow during expansion and osteoblast differentiation. *BMC Genomics* **8**, 70–84
16. Pittenger, M.F., Mackay, A.M., Beck, S.C., Jaiswal, R.K., Douglas, R., Mosca, J.D., Moorman, M.A., Simonetti, D.W., Craig, S., and Marshak, D.R. (1999) Multilineage potential of adult human mesenchymal stem cells. *Science* **284**, 143–147
17. Barrett, T., Troup, D.B., Wilhite, S.E., Ledoux, P., Rudnev, D., Evangelista, C., Kim, I.F., Soboleva, A., Tomashevsky, M., and Edgar, R. (2007) NCBI GEO: mining tens of millions of expression profiles-database and tools update. *Nucleic Acids Res.* **35**, D760–D765
18. Edgar, R., Domrachev, M., and Lash, A.E. (2002) Gene Expression Omnibus: NCBI gene expression and hybridization array data repository. *Nucleic Acids Res.* **30**, 207–210
19. Toda, K., Ishida, S., Nakata, K., Matsuda, R., Shigemoto-Mogami, Y., Fujishita, K., Ozawa, S., Sawada, J., Inoue, K., Shudo, K., and Hayashi, Y. (2003) Test of significant differences with a priori probability in microarray experiments. *Anal. Sci.* **19**, 1529–1535
20. Benini, S., Perbal, B., Zambelli, D., Colombo, M.P., Manara, M.C., Serra, M., Parenza, M., Martinez, V., Picci, P., and Scotlandi, K. (2005) In Ewing's sarcoma CCN3(NOV) inhibits proliferation while promoting migration and invasion of the same cell type. *Oncogene* **24**, 4349–4361
21. Heymans, S., Lupu, F., Terclavers, S., Vanwetswinkel, B., Herbert, J.-M., Baker, A., Collen, D., Carmeliet, P., and Moons, L. (2005) Loss or inhibition of uPA or MMP-9 attenuates LV remodeling and dysfunction after acute pressure overload in mice. *Am. J. Pathol.* **166**, 15–25
22. Mundlos, S., Otto, F., Mundlos, C., Mulliken, J.B., Aylsworth, A.S., Albright, S., Lindhout, D., Cole, W.G., Henn, W., Knoll, J.H.M., Owen, M.J., Mertelsmann, R., Zabel, B.U., and Olsen, B.R. (1997) Mutaions involving the transcription factor CBFA1 cause cleidocranial dysplasia. *Cell* **89**, 773–779
23. Yamamura, Y., Lee, W.L., Inoue, K., Ida, H., and Ito, Y. (2006) RUNX3 cooperates with FoxO3a to induce apoptosis in gastric cancer cells. *J. Biol. Chem.* **281**, 5267–5276
24. Hu, B., Wang, S., Zhang, Y., Feghali, C.A., Dingman, J.R., and Wright, T.M. (2003) A nuclear target for interleukin-1α: Interaction with the growth suppressor necdin modulates proliferation and collagen expression. *Proc. Natl. Acad. Sci. USA* **100**, 10008–10013
25. Chen, C.-J., Kono, H., Golenbock, D., Reed, G., Akira, S., and Rock, K.L. (2007) Identification of a key pathway required for the sterile inflammatory response triggered by dying cells. *Nat. Med.* **13**, 851–856
26. Wan, D., Gong, Y., Qin, W., Zhang, P., Li, J., Wei, L., Zhou, X., Li, H., Qiu, X., Zhong, F., He, L., Yu, J., Yao, G., Jiang, H., Qian, L., Yu, Y., Shu, H., Chen, X., Xu, H., Guo, M., Pan, Z., Chen, Y., Ge, C., Yang, S., and Gu, J. (2004) Large-scale cDNA transfection screening for genes related to cancer development and progression. *Proc. Natl. Acad. Sci. USA* **101**, 15724–15729
27. Herath, N.I., Spanevello, M.D., Sabesan, S., Newton, T., Cummings, M., Duffy, S., Lincoln, D., Boyle, G., Parsons, P.G., and Boyd, A.W. (2006) Over-expression of Eph and ephrin genes in advanced ovarian cancer: ephrin gene expression correlates with shortened survival. *BMC Cancer* **6**, 144–150
28. Woelfle, U., Cloos, J., Sauter, G., Riethdorf, L., Jänicke, F., van Diest, P., Brakenhoff, R., and Pantel, K. (2003) Molecular signature associated with bone marrow micrometastasis in human breast cancer. *Cancer Res.* **63**, 5679–5684
29. Lin, C.G., Chen, C.-C., Leu, S.-J., Grzeszkiewicz, T.M., and Lau, L.F. (2005) Integrin-dependent functions of the angiogenic inducer NOV (CCN3). *J. Biol. Chem.* **280**, 8229–8237
30. Huang, Y., Haraguchi, M., Lawrence, D.A., Border, W.A., Yu, L., and Noble, N.A. (2003) A mutant, noninhibitory plasminogen activator inhibitor type 1 decreases matrix accumulation in experimental glomerulonephritis. *J. Clin. Invest.* **112**, 379–388
31. Sakamoto, K., Yamaguchi, S., Ando, R., Miyawaki, A., Kabasawa, Y., Takagi, M., Li, C.L., Perbal, B., and Katsube, K. (2002) The nephroblastoma overexpressed gene (NOV/ccn3) protein associates with Notch1 extracellular domain and inhibits myoblast differentiation via Notch signalling pathway. *J. Biol. Chem.* **277**, 29399–29405
32. Scherberich, A., Galli, R., Jaquiery, C., Farhadi, J., and Martin, I. (2007) 3D perfusion culture of human adipose tissue-derived endothelial and osteoblastic progenitors generates osteogenic constructs with intrinsic vascularization capacity. *Stem Cells* **25**, 1823–1829

THE JOURNAL OF BIOLOGICAL CHEMISTRY VOL. 283, NO. 31, pp. 21725–21733, August 1, 2008

Ascidian Sperm Glycosylphosphatidylinositol-anchored CRISP-like Protein as a Binding Partner for an Allorecognizable Sperm Receptor on the Vitelline Coat*[S]

Received for publication, April 4, 2008, and in revised form, June 2, 2008 Published, JBC Papers in Press, June 4, 2008, DOI 10.1074/jbc.M802631200

Satoshi Urayama[‡1], **Yoshito Harada**[‡1], **Yoko Nakagawa**[‡1], **Susumu Ban**[‡§], **Mari Akasaka**[‡], **Nana Kawasaki**[¶], **and Hitoshi Sawada**[‡2]

From the [‡]Sugashima Marine Biological Laboratory, Graduate School of Science, Nagoya University, Sugashima, Toba 517-0004, the [§]Department of Biochemistry, Graduate School of Pharmaceutical Sciences, Hokkaido University, Sapporo 060-1206, and the [¶]Division of Biological Chemistry and Biologicals, National Institute of Health Science, 1-8-1 Kamiyoga, Setagaya-ku, Tokyo 158-8501, Japan

Although ascidians are hermaphroditic, many species including *Halocynthia roretzi* are self-sterile. We previously reported that a vitelline coat polymorphic protein HrVC70, consisting of 12 EGF (epidermal growth factor)-like repeats, is a candidate allorecognition protein in *H. roretzi*, because the isolated HrVC70 shows higher affinity to nonself-sperm than to self-sperm. Here, we show that a sperm 35-kDa glycosylphosphatidylinositol-anchored CRISP (cysteine-rich secretory protein)-like protein HrUrabin in a low density detergent-insoluble membrane fraction is a physiological binding partner for HrVC70. We found that HrVC70 specifically interacts with HrUrabin, which had been separated by SDS-PAGE and transferred onto a nitrocellulose membrane. HrUrabin has an *N*-linked sugar chain, essential for binding to HrVC70. *HrUrabin* mRNA is expressed in the testis but not in the ovary, and the protein appears to be localized on the surface of sperm head and tail. Anti-HrUrabin antibody, which neutralizes the interaction between HrUrabin and HrVC70, potently inhibited fertilization and allorecognizable sperm-binding to HrVC70-agarose. However, no significant difference in the binding ability of HrUrabin to HrVC70 was observed in autologous and allogeneic combinations by Far Western analyses. These results indicate that sperm-egg binding in *H. roretzi* is mediated by the molecular interaction between HrUrabin on the sperm surface and HrVC70 on the vitelline coat, but that HrUrabin *per se* is unlikely to be a direct allorecognition protein.

Ascidians, the invertebrate chordates, are hermaphroditic animals releasing gametes nearly simultaneously during the spawning season. Most ascidians show self-sterility or preference for "non-autologous" (allogeneic) fertilization (1, 2), which appears to be beneficial for the achievement of genetic diversity in the next generation. However, the mechanism of self-sterility during ascidian fertilization is a long-standing enigma. In the early part of the 20th century, Morgan (3–6) studied this problem using the solitary ascidian *Ciona intestinalis*, and found that a barrier against self-fertilization is abolished by the treatment of eggs with weak acid (citrus juice) or protease (pancreatic extract) (3). Because the vitelline coat (VC)[3]-free naked eggs are self-fertile, he proposed that a self/nonself-recognition molecule must reside on the VC or test cells. Later, it was found that only nonself-sperm tightly and specifically bound to the VC of glycerinated eggs in *C. intestinalis* (7). From these results, it is currently believed that a certain allorecognition molecule responsible for self-sterility must reside on the VC.

We have been studying the mechanism of self-sterility using another solitary ascidian, *Halocynthia roretzi*, because a large quantity of readily fertilizable gametes can be easily obtained from this species, which is aqua-cultured in Japan for human consumption (8). Although *H. roretzi* exhibits much more strict self-sterility than *C. intestinalis*, the mode of self-sterility in both species seems to be similar. In *H. roretzi*, the occurrence of a self-fertilization barrier on the VC, but not on the follicle cells, was clearly demonstrated by experiments using "mosaic eggs," whose follicle cells were replaced by those of different individuals (9). As in *C. intestinalis*, mature oocytes but not immature oocytes are self-sterile in *H. roretzi*, and the self-sterility is lost by treatment with acidic seawater (9). Furthermore, the acquisition of self-sterility during oocyte maturation was blocked by trypsin inhibitors, whereas exogenously added trypsin stimulates the acquisition of self-sterility (10, 11). These results led us

* This work was supported in part by Grants-in-aid for Scientific Research (B) 15390023 and 18390022 from Japan Society for the Promotion of Science (JSPS), Scientific Research on Priority Area 15040212, 17028024, and 19044019, Exploratory Research 16659021 and 19659018 from the Ministry of Education, Culture, Sports, Science and Technology in Japan (MEXT) (to H. S.), and by Grants-in-aid for Young Scientists (B) 16770159 and 18770198 from MEXT (to Y. H.). The costs of publication of this article were defrayed in part by the payment of page charges. This article must therefore be hereby marked "*advertisement*" in accordance with 18 U.S.C. Section 1734 solely to indicate this fact.

[S] The on-line version of this article (available at http://www.jbc.org) contains supplemental Fig. S1.

The nucleotide sequence(s) reported in this paper has been submitted to the GenBank™/EBI Data Bank with accession number(s) AB276042 (HrUrabin) and AB276041 (HrUrabin-L).

[1] These authors equally contributed to this paper.

[2] To whom correspondence should be addressed. Tel.: 81-599-34-2217; Fax: 81-599-34-2456; E-mail: hsawada@bio.nagoya-u.ac.jp.

[3] The abbreviations used are: VC, vitelline coat; CRISP, cysteine-rich secretory protein; EGF, epidermal growth factor; EPPS, *N*-(2-hydroxyethyl)piperazine-*N*′-3-propanesulfonic acid; GPI, glycosylphosphatidylinositol; HrTTSP-1, *Halocynthia roretzi* type II transmembrane serine protease-1; LDDIM, low-density detergent-insoluble membrane; PI-PLC, phosphatidylinositol-specific phospholipase C; PR, plant pathogenesis-related 1; SCP, sperm-coating glycoprotein; ESI-MS, electrospray ionization mass spectrometry; RACE, rapid amplification of cDNA ends; PBS, phosphate-buffered saline.

to propose that a putative allorecognition protein might be expressed in immature oocytes as a precursor and that the active form might be generated by a trypsin-like protease, resulting in its attachment to the VC during oocyte maturation. It is also inferred that this putative molecule might be easily extracted from the VC by mildly acidic conditions.

To test this possibility, we compared the components of the VCs from immature oocytes with those from mature oocytes of *H. roretzi* by SDS-PAGE. We found that a 70-kDa VC protein HrVC70, which had been identified as a sperm receptor consisting of 12 epidermal growth factor (EGF)-like repeats (12), appears to be attached to the VC during oocyte maturation and that this protein is easily and almost specifically extracted from the insoluble VC by 1–10 mM HCl (pH 2–3) (13). HrVC70 is converted by a trypsin-like protease from its precursor HrVC120, which contains 13 EGF repeats, a zona pellucida domain, and a transmembrane helix (13). Difference in the binding ability of sperm to the VC between autologous and allogeneic gamete combinations is not obvious in *H. roretzi* (10). However, we found that nonself-sperm shows a significantly higher affinity to HrVC70-immobilized agarose beads than self-sperm (13). In addition, fertilization was more strongly inhibited by the pretreatment of sperm with nonself-HrVC70 than self-HrVC70 (13). Finally, HrVC70 appeared to be a highly polymorphic protein, showing no identical sequence among 10 individuals tested (13). From these results, together with the fact that even a single amino acid substitution is sufficient to affect the molecular recognition between EGF-like repeat-containing molecules such as Notch, Delta, and Serrate (14, 15), we proposed that HrVC70 is a promising candidate for the allorecognition protein, which is responsible for self-sterility.

To gain insights on the molecular mechanism of allorecognition, we have explored a sperm-borne binding partner for HrVC70 by several approaches. We previously reported that a type II transmembrane protease, HrTTSP-1, is a candidate sperm-derived HrVC70-interacting protein as revealed by yeast two-hybrid screening baited with HrVC70 (16). In the present report, we carried out Far Western blot analysis using HrVC70 as a probe, and identified a 35-kDa sperm membrane-associated glycosylphosphatidylinositol (GPI)-anchored protein as a physiological binding partner for HrVC70.

EXPERIMENTAL PROCEDURES

Biological Materials and Preparations of the VC and Low-density Detergent-insoluble Membrane (LD-DIM) Fraction—Spawning of *H. roretzi*, collected near Mutsu Bay in northern Japan, was induced by controlling the seawater temperature and light conditions as described previously (17). Sperm and eggs were collected individually and used for fertilization experiments or stored at −20 °C until use.

The VC of *H. roretzi* eggs was prepared as described previously (12). Briefly, frozen-thawed eggs were mixed with an equal volume of homogenizing buffer (20 mM EPPS (pH 8.0), 460 mM NaCl, 10 mM KCl, 1 mM phenylmethylsulfonyl fluoride, and 10 μg/ml leupeptin), and homogenized with a Teflon homogenizer at 2,000 rpm, 10 times. The homogenate was filtered through a nylon mesh (50 μm), and the VC on the mesh was washed with 0.2× artificial seawater 5–10 times, followed by centrifugation at 7,000 × *g* for 5 min. The VC (precipitate) was further washed twice with MilliQ water.

HrVC70 was isolated from the VC as follows (12). The VC was mixed with 2–3 volumes of 10 mM HCl and incubated at 13 °C for 15 min. After centrifugation (15,000 × *g* for 15 min), the supernatant fraction, which contains almost exclusively HrVC70, was neutralized with 50 mM Tris/HCl (pH 8.0) and stored frozen until use.

The LD-DIM fraction from *H. roretzi* sperm was prepared as described previously for sea urchin sperm (18, 19). Briefly, intact sperm suspensions were mixed with an equal volume of homogenizing buffer (10 mM Tris/HCl (pH 7.5), 0.15 M NaCl, 5 mM EDTA, 1% Triton X-100, 1 mM phenylmethylsulfonyl fluoride, and 10 μg/ml leupeptin). After standing for 20 min on ice, the sperm suspension was disrupted with a Teflon homogenizer at 2,000 rpm, 10 times, and subjected to low-speed centrifugation (7,000 ×*g* for 5 min). One ml of the resulting supernatant was mixed with an equal volume of 85% (w/v) sucrose and transferred into an ultracentrifuge tube, which was gently overlaid by 2 ml of 30% sucrose, and 1 ml of 5% sucrose in this order. After centrifugation (200,000 × *g*, 18 h, 4 °C), the LD-DIM fraction was obtained in a boundary between the 5 and 30% sucrose layers. Protein concentration in each fraction separated by ultracentifugation was determined using the ABC kit (Bio-Rad).

Molecular Biological Techniques—Degenerate primers were designed based on the determined N-terminal 30 amino acid residues (forward-1 primer, 5′-GA(A/G)GTN(A/C)GIAT(A/C/T)(C/T)TIACIAC-3′, forward-nested primer, 5′-GA(A/G)GTN(A/C)GIAT(A/C/T)(C/T)TIACIACIGA(A/G)GA(A/G)AA(A/G)CA-3′; I, inosine), and 3′-RACE PCR was performed on gonad cDNA from a reproductively mature animal prepared with the SMART RACE cDNA amplification kit (Clontech). Nearly entire cDNA fragments were obtained by screening a *H. roretzi* gonad λ-ZAP cDNA library (Stratagene) probed with the 3′-RACE product. The 5′ terminus of the mRNA was determined by 5′-RACE.

Northern blotting and genomic Southern blotting of HrUrabins were carried out as described previously (14), using a digoxigenin-labeled cDNA probe corresponding from Pro^{49} to Leu^{287} in *HrUrabin-L*. Whole mount *in situ* hybridization was performed as described previously (16), using a digoxigenin-labeled RNA probe including the entire cDNA sequence of *HrUrabin-L*.

Immunological Procedures and Far Western Analysis—To develop an anti-HrVC70 polyclonal antibody, the HrVC70 band purified from the VC by SDS-PAGE, was used as an antigen. As to HrUrabin, thioredoxin-tagged fusion protein, including the entire sequence of the processed form of HrUrabin-L, was bacterially expressed using the PET Trx Fusion System 32 (Novagen). The rabbit antisera raised against HrVC70 and HrUrabin were prepared by Hokudo Ltd. Anti-HrVC70 antibody specifically reacted to HrVC70 among the VC components, and showed no cross-reactivity to any sperm membrane proteins on the basis of Western blotting under the conditions tested.